ARCHIVES OF ACOUSTICS
1, 3, 181-200 (1976)

FLOW PATTERNS AND NOISE OF A CHOKED GAS JET EXPANDING INTO A DUCT

KRYSTYNA J. WITCZAK

Department of Aerodynamics, Warsaw Technical University (Warsaw)

Axi-symmetric, choked air outflow into a duct with an abrupt enlargement of its cross-section was investigated in order to establish the relations between the flow pattern and the aerodynamic noise generated. Four main kinds of flow structure, possessing different acoustic properties, were found in the cases studied of the outflow from convergent circular and annular nozzles. These patterns correspond to the occurrence of: cellular structure, self-excited oscillations, single shock wave (noise minimum) and supersonic flow. An acoustic feedback type source of sound can appear under certain circumstances in the cellular structure. The self-excited shock wave and pressure oscillations produce noise characterized by discrete frequencies in the sound pressure level spectrum. The reasons for the minimum noise generation, which takes place before the reattachment of the supersonic stream boundary to the duct wall, are explained. Prevention of strong oscillations by the insertion of spoilers at the nozzle lip reduces the noise significantly over a wide range of supply pressures, however it increases the noise minimum due to turbulence intensity growth. Recommendations for nozzle and duct geometry for noise reduction are given.

1. Introduction

In high-pressure industrial installations the gas outflows from the slits of reducing valves and the inflows into ducts with an abrupt enlargement of their cross-section are predominantly choked. This means that the flow velocity at the nozzle exit is equal to the sound speed and an excess in gas pressure causes further jet expansion, the flow velocity in the duct thus attaining supersonic values.

Observation of installations shows that these flows can be a source of strong pressure oscillations and of high intensity noise with characteristic discrete frequencies in its spectrum. These are all unwanted and harmful effects, since the flow oscillations disturb technological processes, make the measurement of flow parameters difficult and produce mechanical vibrations. The noise, which accompanies them, causes the work circumstances for the operating

personnel of such installations to be uncomfortable. For successful prevention of the flow oscillations a study of the phenomenon is necessary.

A survey of published work, connected with noise from choked gas outflows, showed that sound generation by free jets has been investigated rather thoroughly. However there are few papers devoted to outflows into a duct and they are not profound.

It is well known that in a subsonic free jet the most effective emitter of acoustic power is the mixing region, i.e. an intensely turbulent shear-layer between the central uniform jet core and the ambient air [1, 2, 3]. In supersonic flow, new sources of additional noise appear which begin to predominate over the turbulent mixing noise. A free choked gas jet possesses a cellular pattern, formed by expansion, compression and shock waves. The structure of cells and their dimensions depend on the difference between exit and ambient pressure levels.

The noise produced, due to the presence of cells in the stream, results from interactions between turbulent eddies or larger vortices and shock waves [1, 3, 4, 5]. It may be characterized by discrete frequencies in the spectrum, by acoustic feedback (*screech*), or as the noise produced by the same sources, but without feedback, being more broad-band but strongly peaked (*shock associated noise*) [4, 6].

The phenomenon of sound generation by vortex and shock wave interaction is not, as yet, fully explained. It is impossible to estimate theoretically the acoustic power of this type of source in the far field [6, 7].

The second kind of noise, which is characteristic of supersonic flows, takes the form of directional high frequency waves, the so-called Mach waves, emitted by eddies convected downstream on the jet boundary with a supersonic velocity in relation to the ambient sound speed [5, 8]. The source of these waves is located in the supersonic shear-layer near the nozzle.

The acoustic feedback type mechanism is the most effective of all the mechanisms responsible for generating aerodynamic noise. It has been shown that in this case the acoustic efficiency can be as high as 5% [9], whereas in the case of a uniform supersonic jet it does not exceed 0.6% [3]. The screech mechanism has been described by POWELL [10, 11, 12] in the following manner. Under favourable conditions, when the shear-layer on the jet boundary is most susceptible to loss of stability, the acoustic wave generated by the flow is capable of creating a vortex at the nozzle exit. This vortex is amplified in the stream and — when it passes through a shock wave — an acoustic pulse is emitted. Next, the acoustic wave disturbs the stability of the boundary layer at the nozzle exit and this is the source of a new vortex. Thus, the feedback loop is closed. For axi-symmetric screeching jets, the mode of vortices convected downstream is either toroidal [13, 14] or spiral [12, 13, 14]. Similar phenomena have been observed, when a choked gas jet impinges on a flat obstacle [15].

Investigations of the noise generated by flow in a duct have been mostly concerned with ejectors [16, 17], variable cross-section channels [18, 19] and reducing valves [20, 21, 22, 23].

The emission of discrete frequency sound with acoustic feedback was found with a choked outflow from an ejector nozzle [16], just as for free jet. Studies on the axi-symmetric air outflow from a convergent nozzle into a duct with an abrupt enlargement of its cross-section revealed [18, 19] two sources of the discrete frequency noise: one associated with the cellular flow structure, and the second occurring when the normal shock wave was present in the duct. On the basis of the work of JUNGOWSKI [24, 25, 26] and the present author [27], it seems that strong self-excited oscillations of pressure in the dead-air region, accompanied by shock wave oscillations, give rise to the second source of noise. Reports relating to the study of reducing valve noise, contain experimental data about the acoustic power and efficiency of different valve types, and discuss constructional modifications used to attempt to decrease the generated noise level. In order to split the mixing region of the stream outflowing from the valve slit, perforated plates [23] or throttling labyrinths [20] are most often placed at the low-pressure side.

In the investigations of axi-symmetric choked gas outflow into a duct with an abrupt enlargement of its cross-section decribed below, the author was guided by necessity to establish the relationship between the flow pattern and the aerodynamic noise generated. Knowlegde of this relationship should permit such designing of the channels of installations as to lead to a decrease in the acoustic power level emitted.

Notation

AP	amplitude in spectrum of pressure oscillation
D	duct diameter
d	nozzle diameter
d_c	central body diameter of annular nozzle
f	frequency
$OSPL$	overall sound pressure level in [dB] $\Delta OSPL = OSPL - OSPL^*$ [dB]
p	pressure $\overline{p} = p/p_0$, $\overline{p}_0 = p_0/p_0{}^*$
Δp	double amplitude of pressure oscillation
SPL	sound pressure level in [dB] $\Delta SPL = SPL_f - OSPL$ [dB]
φ	ratio of nozzle area to duct area

Suffixes

c	central dead-air region
f	at definite frequency
o	supply
w	outer dead-air region
$*$	appearance of critical outflow from nozzle

2. Outline of experimental studies and measuring technique

The axi-symmetric air outflow from a convergent circular or annular nozzle into a duct with an abrupt enlargement of its cross-section (Fig. 1) was investigated experimentally. The annular nozzle can be regarded as an approximate model of reducing valve. High-pressure air was fed to the supply chamber (1) and the test section (2) was connected with the atmosphere through the set of outlet ducts.

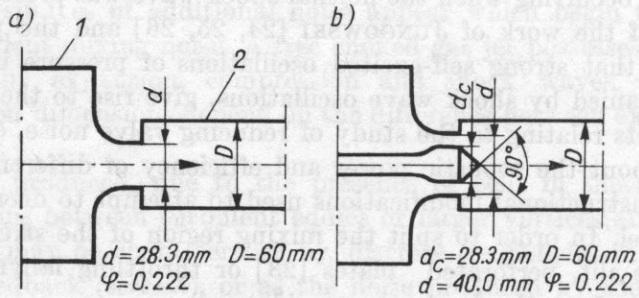

Fig. 1. Circular (a) and annular (b) nozzle arrangements investigated
1 – supply chamber, *2* – test section

The *OSPL* measurements and the spectral-analysis were performed using Brüel and Kjaer equipment. A half-inch microphone was placed in the free field outside the duct, at a distance of 0.4 m away from its axis. Since it was found that the character of the spectra in the neighbourhood of the test section are subject only to minor changes, a representative microphone location was assumed to be a point in the horizontal plane at the height of the duct axis. The microphone was placed at an angle of 45° to the duct axis, and directed towards the nozzle exit, near to which the most powerful sources of noise are located.

The flow patterns were investigated by measurement of: the static pressure distribution along the duct; traces of the oscillating pressure and their associated spectra; flow visualization using schlieren and shadowgraph methods; and streak-pictures (x-t plane). In order to make even a partial visualization possible, a portion of the duct wall, equal in width to half of the diameter, was removed and replaced by flat windows made from optical glass.

3. Flow patterns

The diagrams in Fig. 2 show the nondimensional pressure in dead-air regions downstream of the circular (a) and annular (b) nozzles versus the nondimensional supply pressure, starting from the beginning of critical outflow. In the range of decreasing $\overline{p}_w$ the subsonic stream boundary reattaches to the

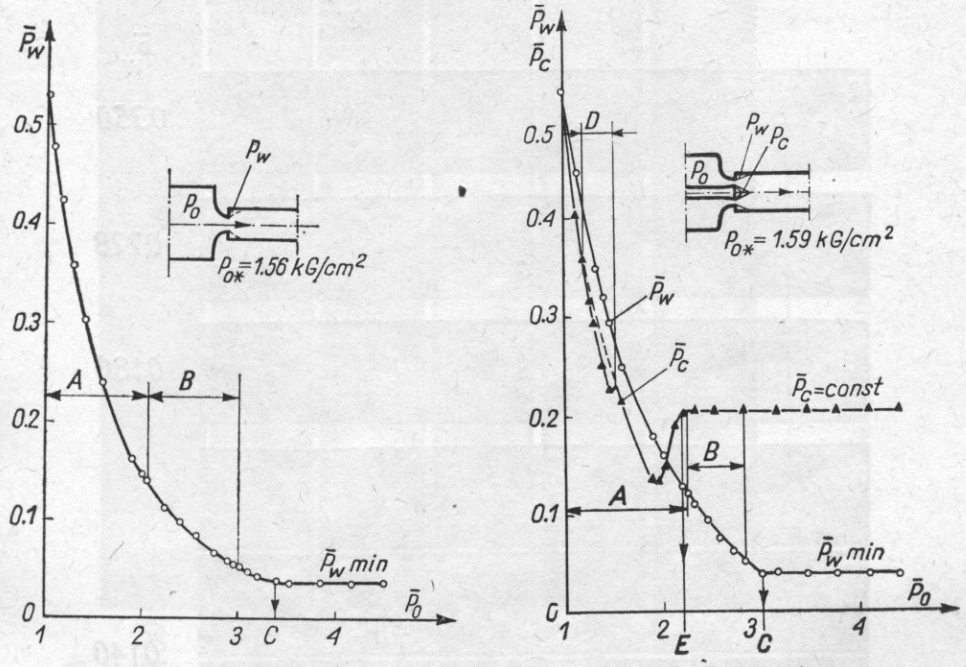

Fig. 2. Nondimensional pressure in outer ($\bar{p}_w$) and central ($\bar{p}_c$) dead-air region versus nondimensional supply pressure ($\bar{p}_0$); choked outflow from circular (a) and annular (b) nozzle into the duct

A – cellular structure, *B* – self-excited oscillations, *C* – supersonic reattachment, *D* – oscillations with acoustic feedback, *E* – closed central dead-air region

duct wall (the so-called *subsonic reattachment*). When the supersonic stream boundary isolates the dead-air region and $\bar{p}_0$ increases, $\bar{p}_w$ maintains its minimum constant value (the so-called *supersonic reattachment*).

At first the flow possesses the features of an underexpanded free jet. The dead-air region is large, since the subsonic stream boundary reattaches to the duct wall a long distance away from the nozzle. The photographs in Fig. 3 and 4a ($\bar{p}_w$ = 0.350-0.180) show the cellular structure of the supersonic region downstream of the circular nozzle, and the photographs in Fig. 4b ($\bar{p}_w$ = 0.400-0.180) show the annular form of the cells in the flow downstream of the annular nozzle.

As the supply pressure further increases, self-excited flow oscillations occur, which are characterized by cyclic variations in flow pattern connected with oscillation of the shock waves and the reattachment zone. Figure 3, for example, shows the changes in flow pattern from a cellular structure to a single shock wave with a frequency of 180 Hz ($\bar{p}_w$ = 0.140), and the changes in shape and position of a single shock wave in the flow oscillating with a frequency of 560 Hz ($\bar{p}_w$ = 0.066).

After the decay of the self-excited flow oscillations ($\bar{p}_w$ = 0.046), before supersonic reattachment, downstream of the single bulging shock wave, near

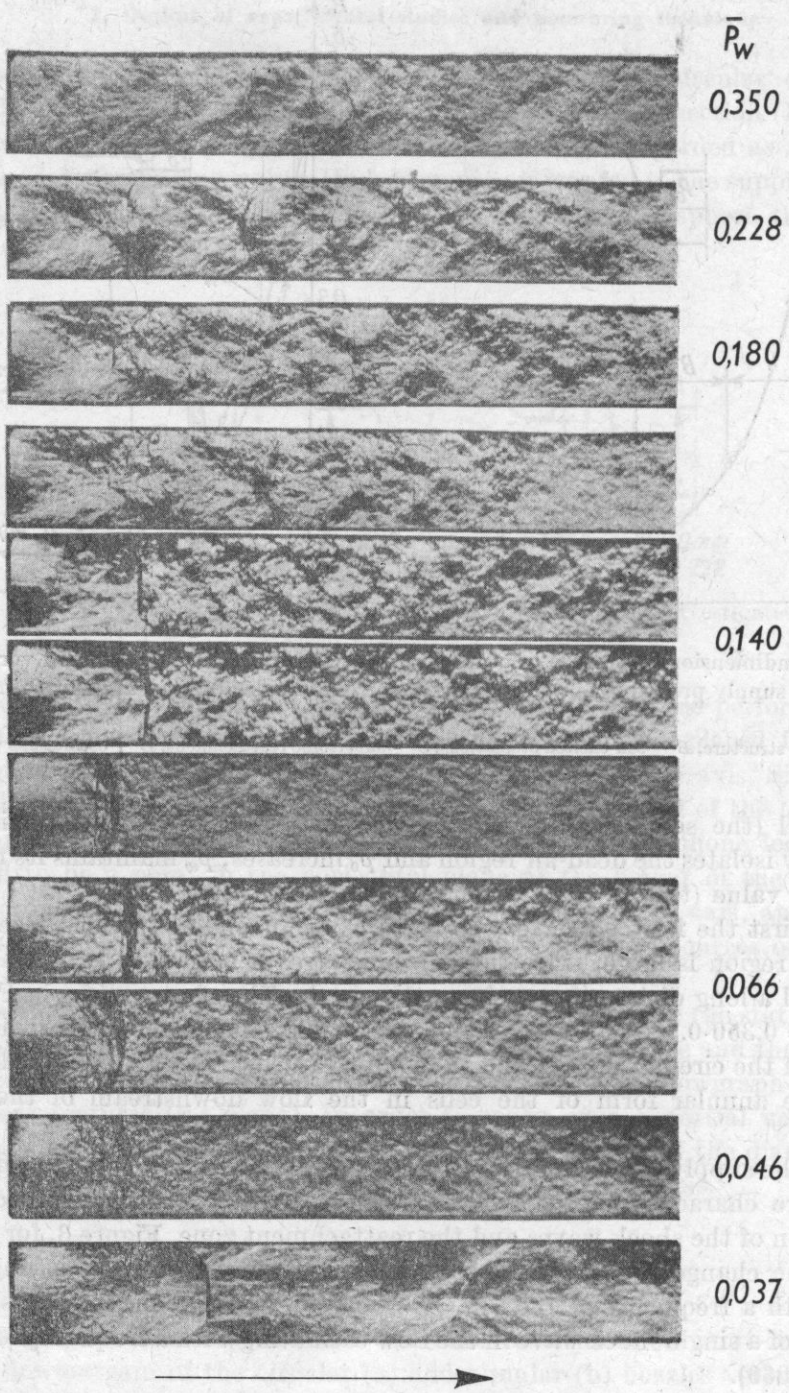

Fig. 3. Schlieren visualization of flow downstream of circular nozzle

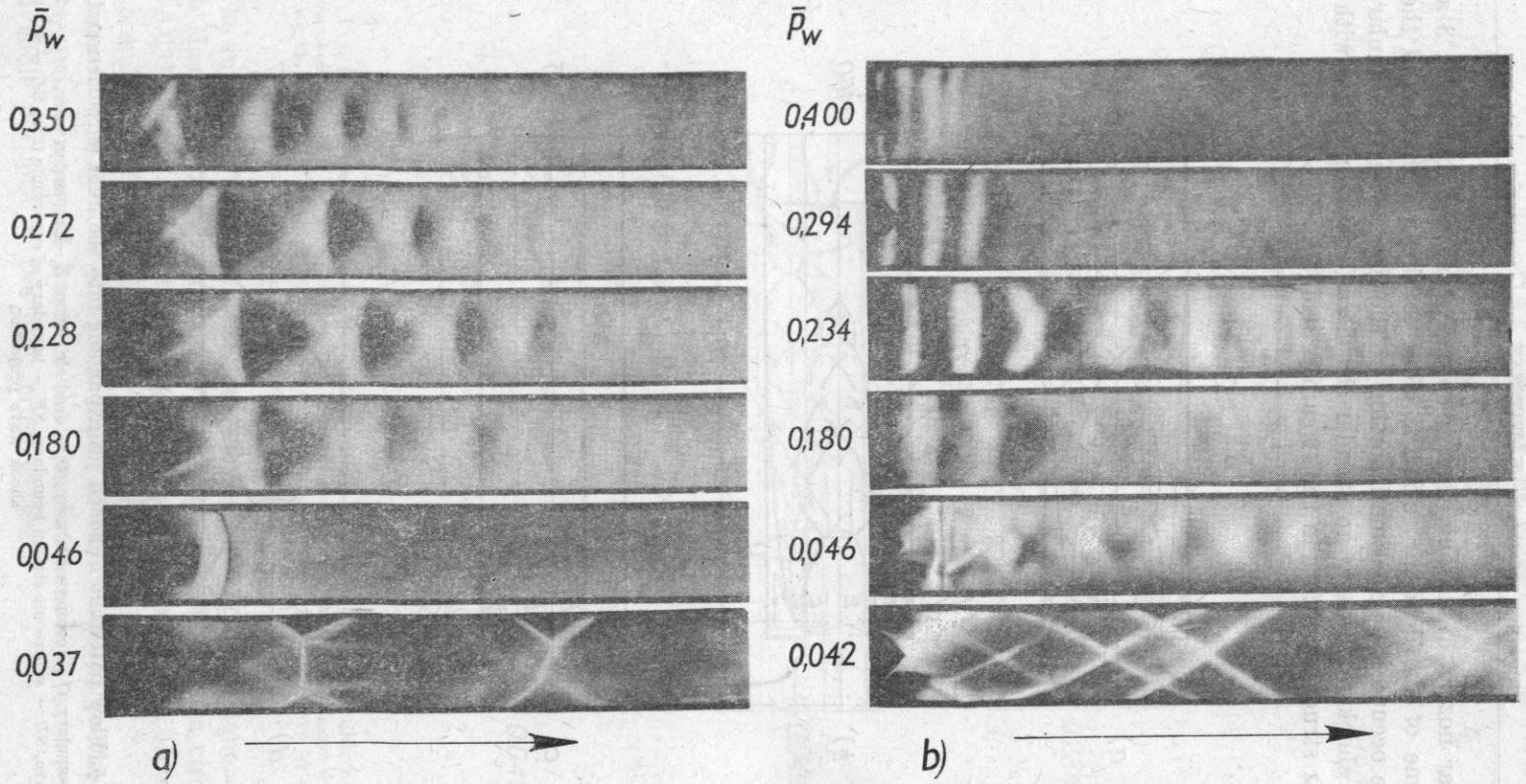

Fig. 4. Schlieren visualization of flow downstream of circular (a) and annular (b) nozzle

the circular nozzle, a subsonic flow is spread along the duct (Fig. 3 and 4a). The volume of the dead-air region is close to the minimum, and the supersonic zone occupies a very small portion of the duct. For the annular nozzle, the single shock wave takes an annular shape and supersonic flow with a typical cellular structure occurs in the stream centre (Fig. 4a).

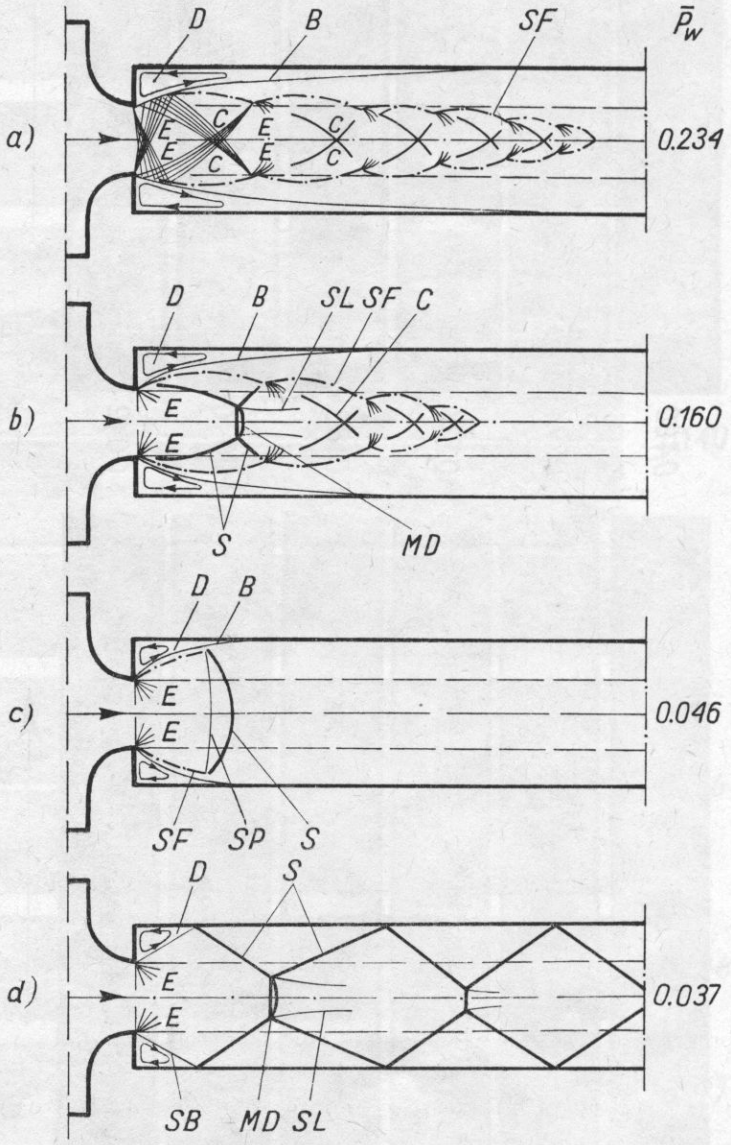

Fig. 5. Flow patterns of choked jet expanding into the duct (circular nozzle)

B – stream boundary, *C* – compression wave, *D* – dead-air region, *E* – expansion wave, *MD* – Mach disk, *S* – shock wave, *SB* – supersonic stream boundary, *SF* – boundary of supersonic flow, *SL* – slip line, *SP* – shock wave projection

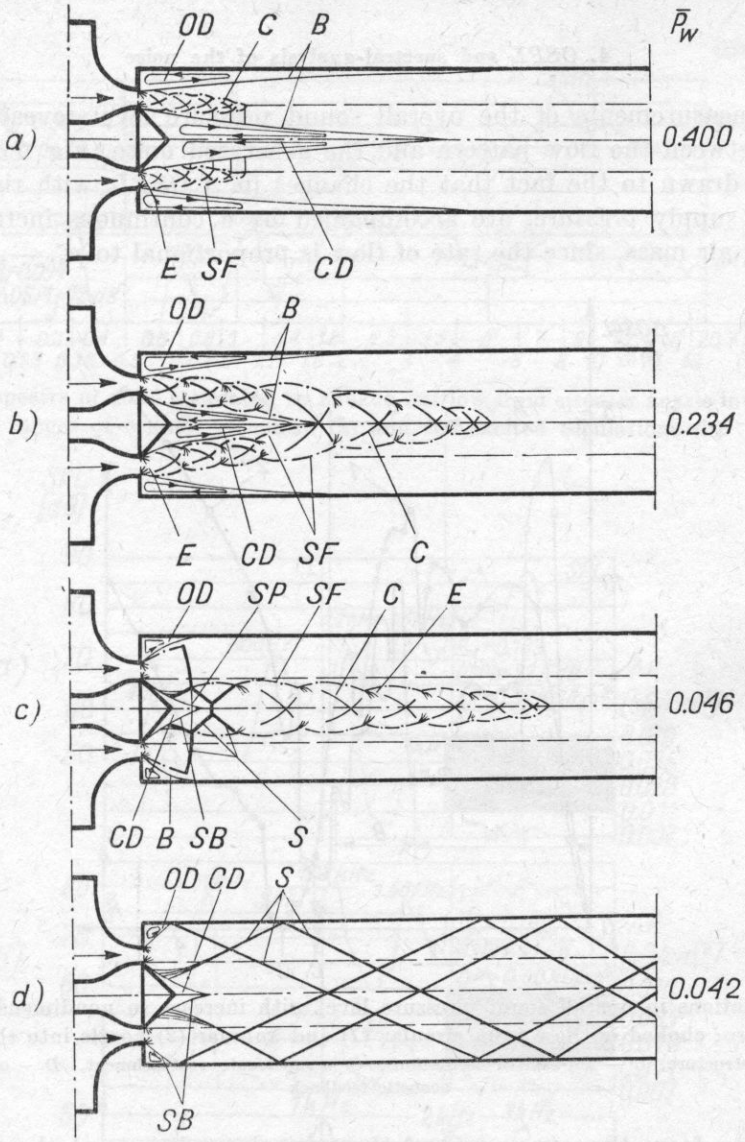

Fig. 6. Flow patterns of choked jet expanding into the duct (annular nozzle)
B – stream boundary, *C* – compression wave, *CD* – central dead-air region, *E* – expansion wave, *OD* – outer dead-air region, *S* – shock wave, supersonic stream boundary, *SF* – boundary of supersonic flow, *SP* – shock wave projection

The supersonic reattachment causes the occurrence of oblique shock waves with a Mach disk (Figs. 3 and 4a) in the flow downstream of a circular nozzle ($\bar{p}_w = 0.037$), and a set of intersecting oblique shock waves (Fig. 4b) downstream of an annular nozzle ($\bar{p}_w = 0.042$).

Figures 5 and 6 show the main kinds of flow patterns (without unstable processes) drawn on the basis of the visualization, with extrapolation over the invisible portions of the duct cross-section.

4. *OSPL* and spectral-analysis of the noise

The measurements of the overall sound pressure level revealed a strict relation between the flow pattern and the generated noise (Fig. 7). Attention should be drawn to the fact that the changes in Δ *OSPL*, with rising nondimensional supply pressure, are accompanied by a continuous increase in the outflowing air mass, since the rate of flow is proportional to p_o.

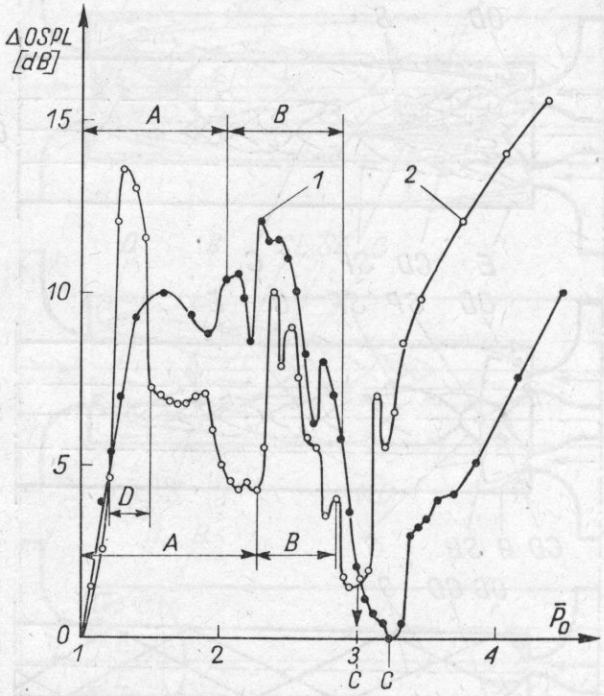

Fig. 7. Variations in overall sound pressure level with increase in nondimensional supply pressure; choked outflow from circular (*1*) and annular (*2*) nozzle into the duct
A – cellular structure, *B* – self-excited oscillations, *C* – supersonic reattachment, *D* – oscillations with acoustic feedback

Starting from the occurrence of the critical conditions at the nozzle exit, in the range of the cellular structure, the noise level increases – in the beginning almost linearly – and then this increase stops. The strong noise maximum ($\bar{p}_0 \approx 1.3$) in the case of the outflow from an annular nozzle is related to the appearance of the particularly effective (acoustic feedback) source of sound with discrete frequencies (3.2 and 6.4 kHz in the spectrum in Fig. 14a). This type source was not observed in the flow downstream of the circular nozzle, but the peak in the spectrum at about 7.3 kHz (Fig. 8a) indicates the sound generated by the interaction of flow disturbances and shock waves.

When the shock waves in the first cell become stronger (Mach disk), the noise diminishes and only self-excited flow oscillations cause an increase

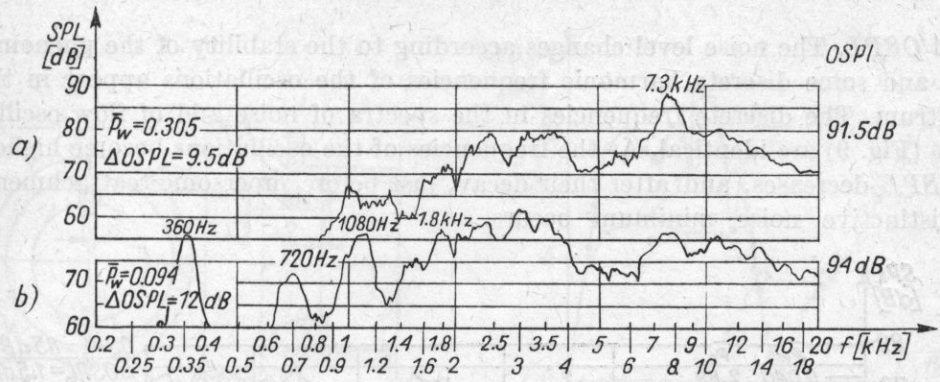

Fig. 8. *SPL* spectra of noise generated by choked outflow from circular nozzle into the duct; ranges of cellular structure (a) and self-excited oscillations (b)

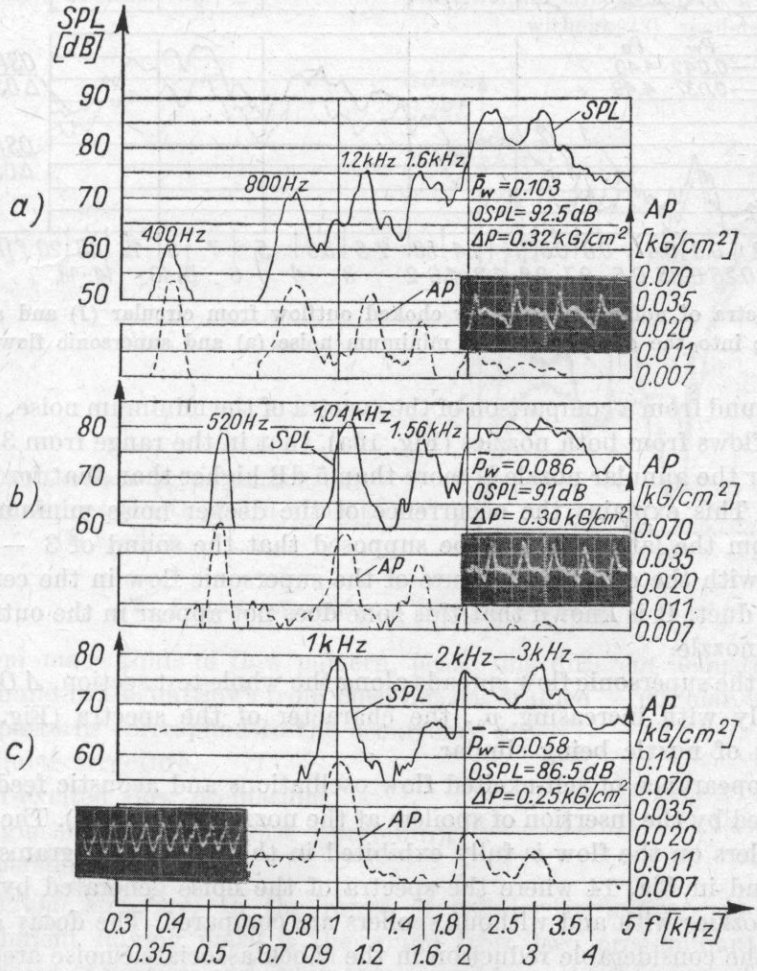

Fig. 9. Spectra of noise (*SPL*) and flow pulsation (*ΔP*) in the range of self-excited oscillations (annular nozzle)

in Δ *OSPL*. The noise level changes according to the stability of the phenomenon and some discrete harmonic frequencies of the oscillations appear in the spectrum. The discrete frequencies in the spectra of noise and of flow oscillations (Fig. 9) are identical. As the frequencies of the oscillations become higher, Δ *OSPL* decreases, and after their decay, just before supersonic reattachment, a distinctive noise minimum occurs.

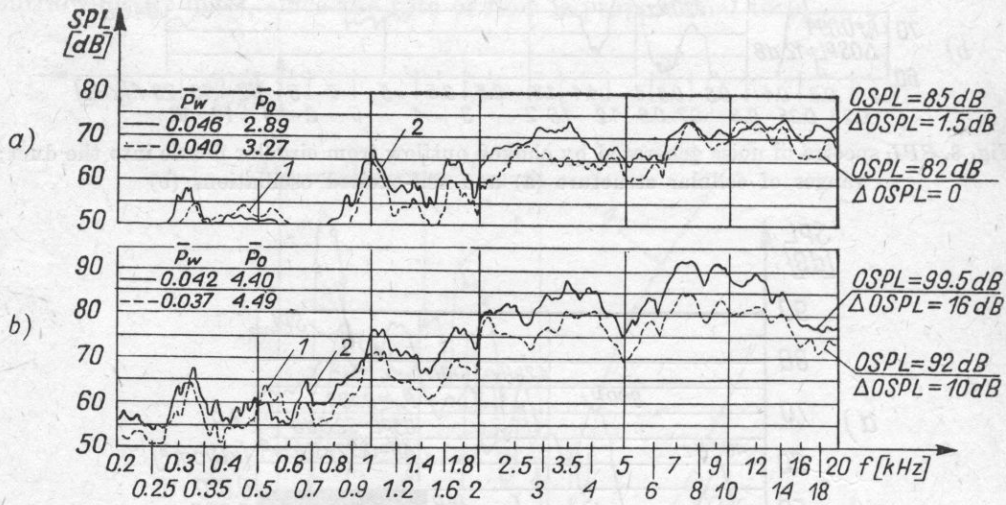

Fig. 10. Spectra of noise generated by choked outflow from circular (*1*) and annular (*2*) nozzle into the duct; ranges of minimum noise (a) and supersonic flow (b)

It is found from a comparison of the spectra of the minimum noise, generated by the outflows from both nozzles (Fig. 10a), that in the range from 3 to 4 kHz the *SPL* for the annular nozzle is more than 5 dB higher than that for the circular nozzle. This explains the occurrence of the deeper noise minimum at the outflow from the latter. It may be supposed that the sound of 3 — 4 kHz is connected with the cellular structure of the supersonic flow in the central portion of the duct. It is known that this zone does not appear in the outflow from a circular nozzle.

When the supersonic flow spreads along the whole test section, Δ *OSPL* rises continuously with increasing $\bar{p}_0$, the character of the spectra (Fig. 10b) for both types of nozzle being similar.

The appearance of self-excited flow oscillations and acoustic feedback can be prevented by the insertion of spoilers at the nozzle lip (Fig. 11). The influence of the spoilers on the flow is fully exhibited in the Δ *OSPL* diagrams (Figs. 12 and 13), and in Fig. 14 where the spectra of the noise generated by outflows from the nozzles with and without spoilers are compared. The decay of oscillations and the considerable reduction in the shock associated noise are, unfortunately, accompanied by an increase in the minimum noise level due to the growth of turbulence intensity.

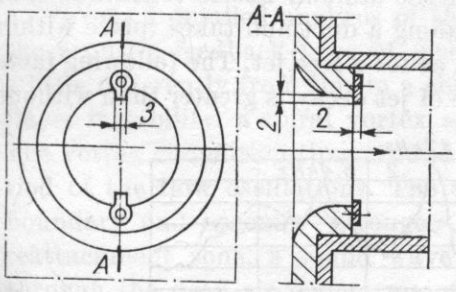

Fig. 11. Dimensions and arrangement of spoilers at nozzle lip

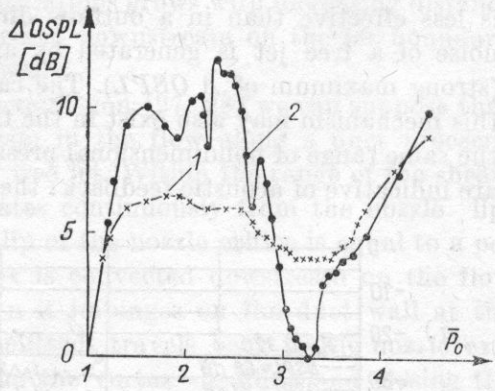

Fig. 12. $\Delta OSPL$ versus $\bar{p}_o$ for choked outflow from circular nozzle with (*1*) and without (*2*) spoilers

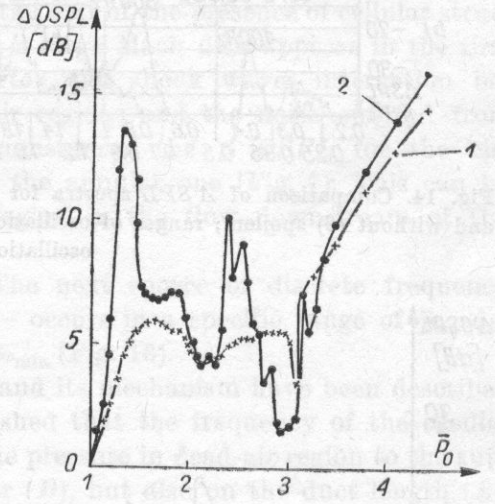

Fig. 13. $\Delta OSPL$ versus $\bar{p}_o$ for choked outflow from annular nozzle with (*1*) and without (*2*) spoilers

5. Acoustic properties of the flow patterns

The four main kinds of flow pattern, possessing different acoustic properties, were found in the outflows from both nozzles studied — circular and annular. These patterns correspond to the occurrence of:

(a) cellular structure,
(b) self-excited flow oscillations,
(c) single shock wave (noise minimum),
(d) supersonic flow.

5.1. *Cellular structure.* In the range of cellular structure, superimposed on the turbulent mixing noise is the sound from two predominant sources: from interaction of vortices and shock waves, and from the flow in large dead-air regions. The source of the shock associated noise in the outflow into the duct

is less effective than in a outflow directly to the atmosphere (Fig. 15). The noise of a free jet is generated by an acoustic feedback type of mechanism (strong maximum of $\Delta\ OSPL$). The case of the annular nozzle confirmed that this mechanism may also exist in the flow along a duct and takes place within the same range of nondimensional pressures as for a free jet. The following facts are indicative of acoustic feedback: the rate of jet decay is greater than without

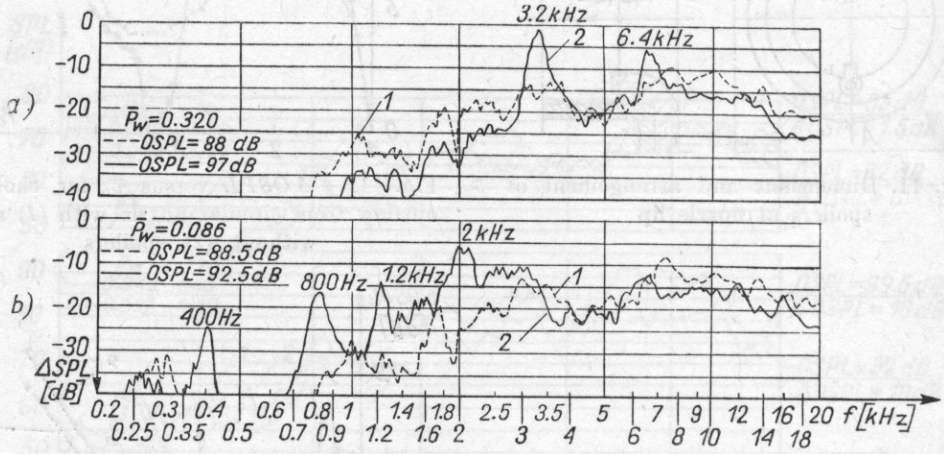

Fig. 14. Comparison of $\Delta\ SPL$ spectra for choked outflow from annular nozzle with (*1*) and without (*2*) spoilers; ranges of oscillations with acoustic feedback (a) and self-excited oscillations (b)

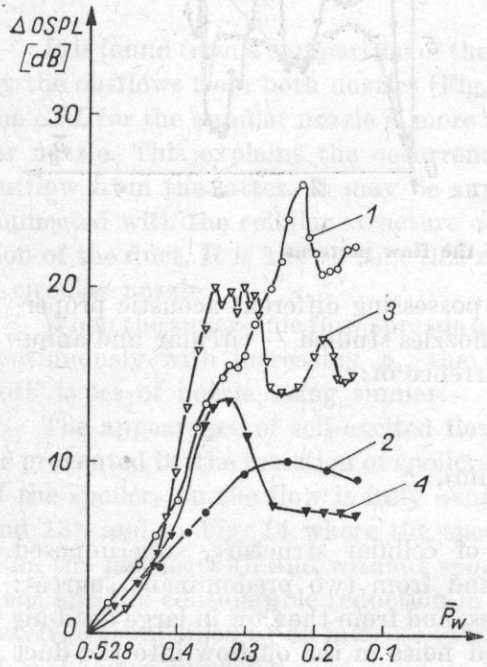

Fig. 15. Comparison of $\Delta\ OSPL$ versus $\bar{p}_w$ for free jets and outflows into duct

Circular nozzle: free jet (*1*), outflow into duct (*2*), annular nozzle: free jet (*3*), outflow into duct (*4*)

oscillations, the amplitude of the flow oscillations grows with increasing distance from the nozzle, disturbances are convected downstream on the jet boundary and decay after impinging on the duct wall.

From a detailed analysis of the phenomenon [27, 28] we can suppose that the acoustic feedback type of mechanism in the flow along a duct proceeds a little differently from this in a choked free jet. Within the range of the shear-layer instability, a spiral vortex separates continuously from the nozzle lip. The vortex circulation-time around the lip of the nozzle orifice is equal to a period of the flow oscillations. The vortex is convected dowstream on the flow boundary and becomes stronger. When it impinges on the duct wall at the reattachment zone, a sound wave is emitted, travels back to the nozzle exit through the dead-air region, maintaining the vortex shedding and closing the feedback loop.

The mechanism described above is rather similar to the situation when a choked gas jet impinges on an obstacle [15].

At a value of $\overline{p}_w$ corresponding to the end of the presence of cellular structure, when a shock wave pattern with a large Mach disk appears in the first cell, Δ *OSPL* diminishes, since the vortex and shock waves interaction becomes weaker. In addition, the dead-air regions and the noise emitted from them are reduced. Under these circumstances the Δ *OSPL* for the circular nozzle is a little higher than for the annular one (Fig. 7). This can be explained by the shorter supersonic region in the flow downstream of the latter nozzle.

5.2. *Self-excited flow oscillations.* The next source of discrete frequency noise — self-excited flow oscillations — occurs in a specific range of $\overline{p}_w$, depending on φ, in the neighbourhood of $\overline{p}_{w\min}$ (Fig. 16).

Investigations of the phenomenon and its mechanism have been described in detail elsewhere [27]. It was established that the frequency of the oscillations depends not only on the ratio of the pressure in dead-air region to the supply pressure ($\overline{p}_w$) and the duct diameter (D), but also on the duct length (L). Among others, we find sudden changes in the oscillation frequency and ranges of evident instability of both amplitude and frequency. When the exciting frequency is close to the frequency of natural gas oscillations in the duct, the flow oscillations are amplified. In this case maxima appear in the diagram of Δ *OSPL* versus $\overline{p}_0$.

The essence of the mechanism of self-excited flow oscillations is as follows. Under some conditions the equilibrium of the dead-air region can be disturbed, i.e. the mass flow ejected from the dead-air region ceases to be equal to the mass flow reversed back into it from the reattachment zone. The flow separates from the duct wall, and changes in the magnitude of the dead-air region and shock wave oscillation occur. The time-varying effects in the dead-air region vary the boundary conditions of the main flow and this results in a fluctuation of flow parameters. The dead-air region and main flow interaction is delayed

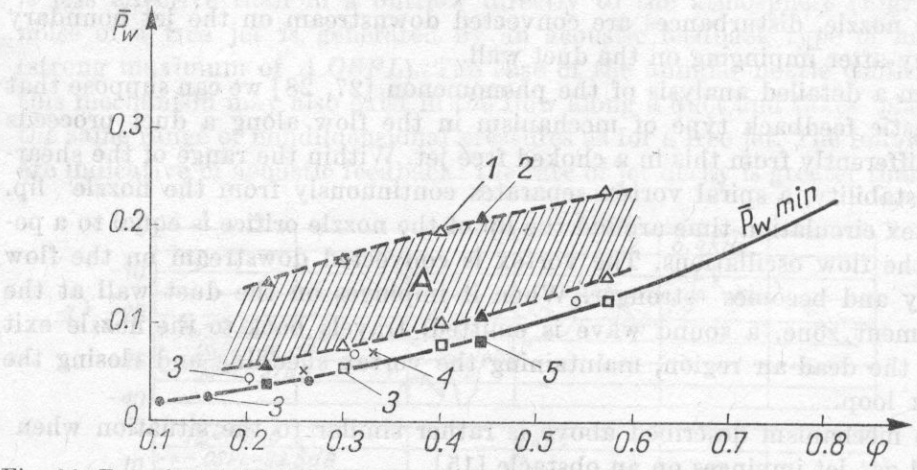

Fig. 16. Experimental values of $\bar{p}_w$ for range of self-excited oscillations and for supersonic reattachment ($\bar{p}_{w_{min}}$)

A – range of self-excited oscillations, *1* – from [25], *2* – from [27], $p_{w_{min}}$, *3* – from [25], *4* – from [18, 19], *5* – from [27]

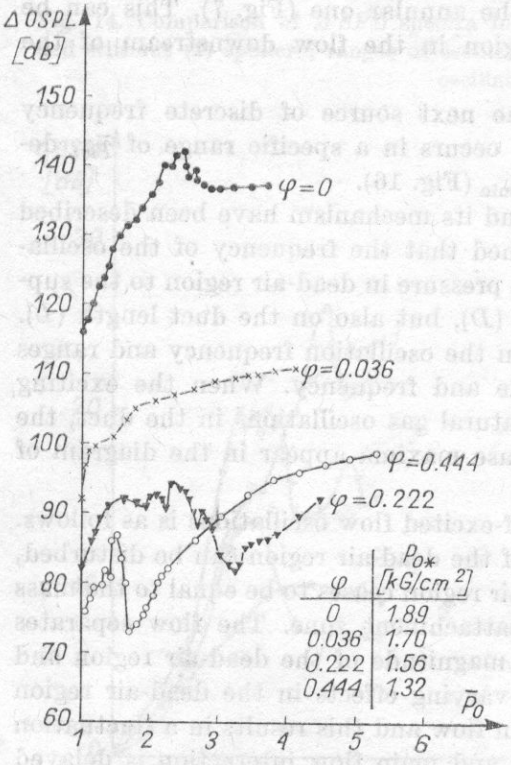

Fig. 17. Comparison of *OSPL* versus $\bar{p}_0$ for outflows from circular nozzle into various φ ducts and to the atmosphere ($\varphi = 0$)

due to inertial effects (for instance — the upstream motion of compression or expansion waves) preventing the formation of equilibrium between these two regions and maintaining unsteady processes.

When the self-excited flow oscillations appear, the low frequency sound — in a range of frequencies up to about 3 kHz — contributes more to the noise spectrum (Fig. 14b).

With a rise in the supply pressure the frequencies of oscillations increase, while changes in the flow pattern become weaker. Thus the amplitudes of oscillations diminish and, moreover, the dead-air region and the zone of supersonic flow are contracted. Owing to the influence of all these factors the Δ *OSPL* displays a tendency to reduce.

5.3. *Single shock wave* (*noise minimum*). The most advantageous flow pattern — from the point of view of the noise generation — occurs in the duct after the decay of self-excited oscillations. It is evident from Fig. 7 that the reduction in Δ *OSPL* in the case of a circular nozzle is very strong, because it reaches — in spite of an almost triple increase in the mass rate of flow — the level recorded at the beginning of critical outflow from the nozzle. The noise minimum appears as a result of a considerable flow velocity reduction due to the presence of a single shock wave near the circular nozzle. In these circumstances, the noise spectrum represents, in fact, the broad-band noise of turbulent subsonic flow along the duct, because the supersonic region is minimal.

The minimum noise level for the annular nozzle is 1.5 dB higher than for the circular nozzle owing to the fact that the shape of shock wave is annular and supersonic flow occupies the central portion of the duct.

A flow structure with similar acoustic properties (noise minimum) was obtained as a result of the interaction of two co-axial supersonic jets — circular and annular [29]. Its characteristic feature was also a minimal supersonic region due to the formation of a shock wave pattern near the nozzle in both jets. It was estimated that the contribution of the supersonic region to the emission of acoustic power was less than 1 %, almost all the noise being generated by the subsonic mixing region of the jets.

5.4. *Supersonic flow.* When the supersonic stream boundary reattaches itself to the wall, supersonic flow with a system of oblique shock waves appears in the duct. The supersonic region spreads downstream along the duct as the supply pressure grows, but the Mach number on the stream boundary and the flow pattern near the nozzle remain unchanged. The noise in this range increases continuously. The difference between the Δ *OSPL* levels (Fig. 7) just after the supersonic reattachment, can be explained by some dissimilarity of the flow structures downstream of the nozzles. The shock wave pattern in the case of the circular nozzle exhibits Mach disks, thus in a small region the flow is subsonic. On the other hand, downstream of the annular nozzle the set of intersecting oblique shock waves is doubled; shocks are formed in the reattachment

zone at the duct wall and at the boundary of the central dead-air region in the place where the flow direction is changed. The progressive rise in Δ *OSPL* is, however, similar for both nozzles.

6. Conclusions

The noise generated by choked gas outflow into a duct with an abrupt enlargement of its cross-section is closely connected with the type of flow pattern. As the supply pressure grows, cellular structure, self-excited flow oscillations, single shock wave and supersonic flow occur consecutively in the duct downstream of the nozzle.

In the flow along the duct acoustic feedback can appear, but it is impeded and less effective than in a free jet, its mechanism differing a little from the «screech» mechanism. In order to fully understand the phenomenon of acoustic feedback in the flow along the duct, the conditions necessary for its presence should be established. We can suppose that since the vortex has to impinge on the duct wall under favourable circumstances in order to emit an acoustic wave, which closes the feedback loop, this phenomenon cannot appear for both small and large φ. In the first case, the vortex decays before arriving at the wall, and in the second case it impinges on the duct wall before it has been appropriately amplified.

The investigations performed revealed that flow oscillations — of both acoustic feedback and self-excited types — are the most effective noise sources in the range of $\overline{p}_w$ up to supersonic reattachment. The discrete frequencies in the spectra of the noise generated, when these two types of oscillations are present, agree completely with the frequencies of pressure oscillations in the flow. Under such circumstances a spectral analysis of the sound recorded in the free field outside the duct could be helpful in determining the frequencies of the flow oscillations.

The most favourable flow circumstances, characterized by the emission of minimum acoustic power, occur in the duct just before supersonic reattachment, when the single shock wave near the nozzle causes a considerable reduction in flow velocity.

The insertion of spoilers at the nozzle exit prevents strong flow oscillations, diminishing the noise in a wide range of supply pressures. It does, however, increase its minimum value before supersonic reattachment due to the growth of turbulence intensity.

The main conclusions of practical significance to be drawn from this work, are as follows.

The more the outflow into the duct is similar to a free jet (small values of φ), the stronger is the shock associated noise and the noise emitted from the dead-air region.

For a high φ the supersonic stream boundary reattaches to the duct wall at a low supply pressure. In view of the noise generation supersonic flow along the duct is undesired.

In the case of devices having little change of supply pressure, the geometrical dimensions of the nozzle and the duct should be chosen in such a way that the operating conditions correspond to the noise minimum. These conditions can easily be established since they occur just before $\overline{p}w_{\min}$. It is more purposeful to select the lower values of φ, e.g. of the order of 0.2 to 0.3, because the range of the noise minimum is wider for these values and, moreover, because the appearance of supersonic reattachment requires a higher change in the supply pressure.

If the supply pressure of the installation is varied over a wide range, the ratio of the nozzle area to the duct area should be so selected that $\overline{p}w_{\min}$, and thus supersonic flow along the duct, are avoided. Strong flow oscillations can be prevented by the insertion of spoilers at the nozzle exit. In this case, the device is characterized by an almost constant noise level, in spite of large changes in the supply pressure.

Acknowledgements. The author wishes to thank Dr. W.M. JUNGOWSKI for suggesting this problem and for his helpful advice, and colleagues G. SOBIERAJ and J. BOJAKOWSKI for help in performing the measurements.

References

[1] M.J. LIGHTHILL, *Sound generated aerodynamically*, The Bakerian Lecture 1961 Proceedings of the Royal Society of London, Series A, **267**, 147-182 (1962).

[2] H.S. RIBNER, *The generation of sound by turbulent jets*, Academic Press, Advances in Applied Mechanics, **8**, 103-182 (1964).

[3] M.J. LIGHTHILL, *Jet noise*, AIAA Journal, **1**, 7, 1507-1517 (1963).

[4] M.J. FISHER, P.A. LUSH, M. HARPER BOURNE, *Jet noise*, Journal of Sound and Vibration, **28**, 3, 563-585 (1973).

[5] V.M. MAMIN, A.V. RIMSKI-KORSAKOV, *Supersonic air jet as the source of sound* [in Russian], Physics of aerodynamic noise, Publ. SCIENCE, Moscow 1967, p. 77-82.

[6] J.E. FFOWCS WILLIAMS, *Jet noise at very low and very high speed*, Aerodynamic noise, Proceedings of AFOSR-UTIAS Symposium, Toronto 1968, p. 131-146.

[7] J.B. LARGE, J.F. WILBY, E. GRANDE, A.O. ANDERSSON, *The development of engineering practices in jet, compressor, and boundary layer noise*, Aerodynamic noise, Proceedings of AFOSR-UTIAS Symposium, Toronto 1968, p. 43-67.

[8] K.A. BISHOP, J.E. FFOWCS WILLIAMS, W. SMITH, *On the noise sources of the unsuppressed high-speed jet*, Journal of Fluid Mechanics, **50**, 1, 21-31 (1971).

[9] V.M. MAMIN, A.V. RIMSKI-KORSAKOV, *Some properties of discrete sound emission by supersonic air jet*, [in Russian], Proceedings of 7th All-Union Acoustic Conference of Physical and Technical Acoustics, 1971, p. 233-236.

[10] A. POWELL, *Nature of the feedback mechanism in some fluid flows producing sound*, 4th International Congress on Acoustics, Copenhagen 1962, paper 0-22.

[11] A. POWELL, *On the noise emanating from a two-dimensional jet above the critical pressure*, The Aeronautical Quarterly, **4**, 103-122 (1953).

[12] A. POWELL, *On the mechanisms of choked jet noise*, Proceedings of the Physical Society, Section B, **66**, part 12, 408 B, 1039-1056 (1953).

[13] M.G. DAVIES, D.E. OLDFIELD, *Tones from a choked axisymmetric jet*, Acustica, **12**, 4, 257-277 (1962).

[14] R. WESTLEY, J.H. WOOLLEY, *An investigation of the near noise fields of a choked axi-symmetric air jet*, Aerodynamic noise, Proceedings of AFOSR-UTIAS Symposium, Toronto 1968, p. 147-167.

[15] G. NEUWERTH, *Acoustic feedback of a subsonic and supersonic free jet which impinges on an obstacle*, 5th DGLR-Meeting, Berlin 1972.

[16] D. MIDDLETON, E.J. RICHARDS, *Discrete frequency noise from ejector nozzles*, 4th International Congress on Acoustics, Copenhagen 1962, paper L 21.

[17] D. MIDDLETON, *Theoretical and experimental investigations into the acoustic output from ejector flows*, Journal of Sound and Vibration, **11**, 4, 447-473 (1970).

[18] J.S. ANDERSON, T.J. WILLIAMS, *Base pressure and noise produced by the abrupt expansion of air in a cylindrical duct*, Journal of Mechanical Engineering Science, **10**, 3, 262-268 (1968).

[19] J.S. ANDERSON, *The noise from abruptly expanded jets*, EUROMECH 34, Colloquium on Control and Feedback Mechanisms in Flow Noise, Göttingen 1972.

[20] E. KOPPE, E.A. MÜLLER, *Modellversuche zur Klärung von Geräusch- und Vibrationsfragen an Reduzierventilen*, Mitteilungen der Vereinigung der Grosskesselbesitzer, 41, 65-83 (1956).

[21] A. NAKANO, *Characteristics of noise emitted by valves*, 6th International Congress on Acoustics, Tokyo 1968, p. F169-F172.

[22] D.J. SMALL, *Noise of high-pressure gas regulator valves*, 7th International Congress on Acoustics, Budapest 1971, p. 345-348.

[23] K.M. HYNES, *The development of a low-noise constant area throttling device*, ISA Transactions, **10**, 4, 416-421 (1971).

[24] W.M. JUNGOWSKI, *On the pressure oscillating in a sudden enlargement of a duct section*, Fluid Dynamics Transactions, edited by W. Fiszdon, Pergamon Press and PWN, 1967, p. 735-741.

[25] W.M. JUNGOWSKI, *Investigation of flow pattern, boundary conditions and oscillation mechanism in a compressible flow through sudden enlargement of a duct*, The Scientific Journal, Mechanics, No 3, Warsaw Technical University Publications, 1968.

[26] W.M. JUNGOWSKI, *On the flow in a sudden enlargement of a duct*, Fluid Dynamics Transactions, edited by W. Fiszdon, Pergamon Press and PWN, **4**, 231-241 (1969).

[27] K.J. WITCZAK, *Choked gas outflow into a duct as the source of noise* [in Polish], Dr. THESIS, Warsaw Technical University, 1975.

[28] W.M. JUNGOWSKI, K.J. WITCZAK, *Properties of an annular jet generating discrete frequency noise* (to be published).

[29] D.S. DOSANJH, J.C. YU, A.N. ABDELHAMID, *Reduction of noise from supersonic jet flows*, AIAA Journal, **9**, 12, 2346-2353 (1971).

Received 30th January 1976

ARCHIVES OF ACOUSTICS
1, 3, 201-213 (1976)

CORRELATION METHOD OF MEASUREMENTS OF SOUND POWER IN THE NEAR FIELD CONDITIONS

STEFAN CZARNECKI*, ZBIGNIEW ENGEL**,
RYSZARD PANUSZKA**

The results of sound power measurements under near field conditions have been compared with the results obtained for far field conditions. For near field measurements correlation and phase methods were used. Far field conditions were investigated by means of reverberation and free-field methods. The experiments were performed on a piston in an infinite baffle, the situation assumed in the calculations.

Quite good agreement of the results was obtained at low frequencies. For the higher frequencies this agreement appeared to be worse although this disagreement has been explained theoretically.

The usefulness of a correlation method for the measurement of sound power under near field conditions was confirmed. The method can be used in practice for the evaluation of the sound power generated by different parts of machinery.

1. Introduction

One of the main problems of machinery noise is the identification of its sound sources, i.e. the location of the main sound sources of the machine, the determination of their sound power, and finding their frequency response.

In a previous paper [1], the fundamentals of the application of the correlation method to the evaluation of the sound power of vibroacoustical sources were presented. The method was based on the measurement of the cross-correlation function between the mechanical velocity of a vibrating element and the sound pressure in the near-field of its radiation.

* The Department of Aeroacoustics, Institute of Fundamental Technological Research, Polish Academy of Sciences (00-049 Warszawa).

** Institute of Mechanics and Vibroacoustics, Academy of Mining and Metallurgy (30-059 Kraków).

The main errors which can occur in the near-field measurements are: an increase of sound pressure due to reflections between the microphone and the vibrating surface, the influence of the phase shift between velocity and acoustic pressure [2] which is dependent on the distance of the microphone from the vibrating elements and the phase shifts of the measuring channels. Moreover, the investigation of the sound power near the source is intended to restrict the influence of radiation from neighbouring sources on the acoustic pressure being measured. These studies are thus of essential for the quantitative estimation of the acoustic power radiated by particular elements of the machinery or device under test.

The aim of this paper is to compare the results of the estimation of acoustic power using the correlation method in the near-field to the results obtained in the far field using the free field [3, 4] and reverberation methods.

The experiments were performed for a vibrating circular piston placed in a large baffle. This permitted verification of the experimental results by analytical calculations. The calculations were based on theoretical relations [5, 8] and on measurements of the phase shift between the vibration velocity of the source surface and the sound pressure.

2. The acoustic power and characteristic impedance of a piston vibrating in an infinite baffle

The overall sound power of a circular piston vibrating in an infinite baffle can be represented, for a sinusoidal signal, by the expression

$$W_a = \frac{1}{T}\int_0^T \left[\mathrm{Re}\iint_S v_{am} e^{j\omega t} p_{am} e^{j(\omega t+\varphi_{pvt})}\, dS\right] dt, \tag{1}$$

where T — the period of vibration, Re — the real part of the expression, v_{am} and p_{am} — the amplitudes of acoustic velocity and sound pressure near to the piston, respectively, $S = \pi a^2$ — the piston area, a — the radius of piston, φ_{pvt} — the phase shift between the sound pressure and the acoustic velocity. It is the argument of the acoustic impedance Z of the piston, which is given by

$$Z = \frac{\hat{p}_{am}}{\hat{v}_{am}} = |Z| e^{j\varphi_{pvt}} = R_p + jX_w, \tag{2}$$

where R_p — the radiation resistance, X_w — the imaginary part of the piston impedance. The phase shift angle φ_{pvt} can be determined from the relation

$$\varphi_{pvt} = \tan^{-1}\frac{X_w}{R_p}, \tag{3}$$

which requires calculation of the components of the impedance of the piston loading.

In general, it is difficult to calculate the impedance of a piston with a non-uniform distribution of vibration velocity on its surface [6,7]. Assuming one of kinds of the boundary conditions of piston in dependence on the method of its fixing, it is possible to determine the eigenmodes of the piston. For the frequencies of eigenmodes the maximum non-uniformity of velocity distribution will appear. The lowest frequency of an eigenmode should be treated as a limit below which it is possible to assume that the distribution of vibration velocity on the piston surface is approximately constant. These frequencies are

– for a supported piston

$$f_{01} = 0.21 \frac{b}{a^2} \sqrt{\frac{E}{\varrho(1-\nu^2)}}, \tag{4}$$

– for a rigidly fixed piston

$$f_{01} = 0.47 \frac{b}{a^2} \sqrt{\frac{E}{\varrho(1-\nu^2)}}, \tag{5}$$

where b – the thickness of the piston, a – its radius, E – Young's modulus, ϱ – the density, ν – Poisson's ratio.

To eliminate the non-uniformity of the velocity distribution on the piston surface the area of piston can be replaced by an equivalent area S_{eq} with a constant distribution.

For the fundamental eigenmode frequency we have, for a

– supported piston [8]

$$S_{eq} = 0.43\, S, \tag{6}$$

– and for a rigidly fixed piston

$$S_{eq} = 0.29\, S. \tag{7}$$

This means that the level of the sound power radiated by the piston is 3.7 dB lower than the level of the power calculated for a constant velocity distribution over a supported plate, and 5.4 dB lower than for a rigidly fixed plate. It follows that the agreement between the calculated and measured results is attained only below the lowest eigenmode frequency f_{01}.

Neglecting the non-uniformity of the velocity distribution at frequencies near f_{01} and above it, gives too high results for the calculated sound power.

Let us assume that the acoustic velocity v_a at a small distance from the piston surface is equal to the velocity v_0 of the vibrating piston which has a constant velocity distribution.

Then, after integrating expression (1), we obtain the following expression for the real part of sound power radiated by the piston:

$$W_a = \tfrac{1}{2} p_{am} v_m S \cos\varphi_{pvt}. \tag{8}$$

Using (2) and (6), expression (8) can be tranformed to a form convenient for calculations:

$$W_a = \tfrac{1}{2} v_m^2 R_p S. \tag{9}$$

The radiation resistance R_p and phase shift φ_{pvt} can be determined from the well- known formula for the impedance of a piston in an infinite baffle,

$$Z = \varrho_0 c \left[1 - \frac{J_1(2\,ka)}{ka}\right] + j\varrho_0 c \left[\frac{K_1(2\,ka)}{2(ka)^2}\right] = R_p + jX_w, \tag{10}$$

where $k = \omega/c$ — wave number, a — radius of piston, ϱ_0 — air density, c — sound speed, $J_1(2\,ka)$ — Bessel function of the 1st kind and 1st order, $K_1(2\,ka)$ — Rayleigh function.

If $ka < 1$, then

$$R_p = \varrho_0 c \frac{k^2 a^2}{2}, \tag{11}$$

$$X_w = \varrho_0 c \frac{8\,ka}{3\pi}, \tag{12}$$

$$\varphi_{pvt} = \tan^{-1} \frac{16}{3\pi ka}. \tag{13}$$

If $ka > 1$

$$R_p = \varrho_0 c, \tag{14}$$

$$X_w = \varrho_0 c \frac{2}{\pi ka}, \tag{15}$$

$$\varphi_{pvt} = \tan^{-1} \frac{2}{\pi ka}. \tag{16}$$

The level of the real part of the sound power in relation to the reference power $W_0 = 10^{-12}\ W/m^2$ is

$$L_t = 10 \log \frac{W_a}{W_0} = 10 \log \frac{\varrho_0 c}{4} \pi k^2 a^4 v_m^2 \times 10^{12} \quad [\mathrm{dB}] \quad \text{for } ka < 1, \tag{17}$$

and

$$L_t = 10 \log \frac{W_a}{W_0} = 10 \log \frac{\varrho_0 c}{2} \pi a^2 v_m^2 \times 10^{12} \quad [\mathrm{dB}] \quad \text{for } ka > 1. \tag{18}$$

For a constant velocity distribution on the piston surface, the distribution of acoustic pressure near the piston should be constant. At longer distances from the vibrating surface the directional piston characteristics will differ more and more from a hemispherical one as the value of ka increases. This effect

occurs for values of $ka > 1$ and causes a decrease in the mean value of the sound pressure level in the far field. This means that for $ka > 1$ the values of power measured under far field conditions will be smaller than the values for near field conditions.

3. Measuring conditions and testing method

The schematic diagram of the testing arrangement is shown in Fig. 1. It includes: the driving system and the emitting source in the form of a circular piston in a baffle. The piston 1 with a smooth and flat surface is fixed to the

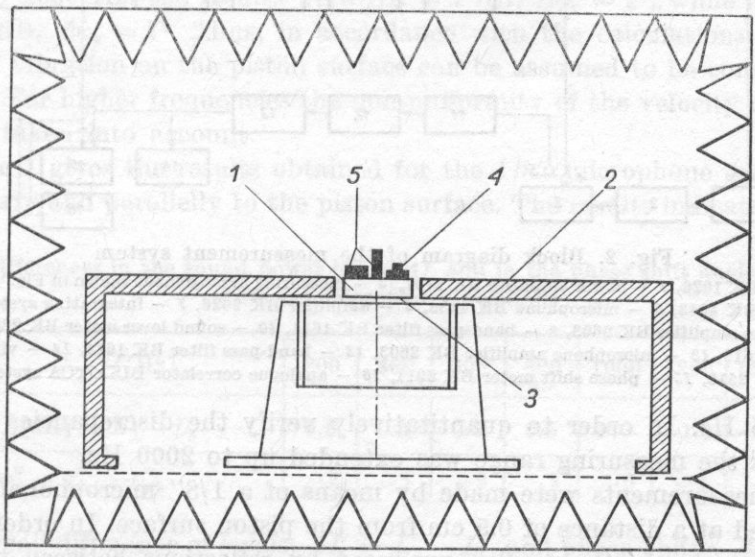

Fig. 1. Schematic diagram of the experimental arrangement for measurements of the acoustic power of a piston in a baffle
1 – piston, *2* – baffle, *3* – driver BK 4801, *4* – acceleration pick-up, *5* – microphone

head of an electrodynamic driver 3 (BK 4801). The driver base is attached to the support structure located in an anechoic chamber. The piston plate forced by the driver head is capable of vibrating in the circular hole of the baffle.

A steel piston with a diameter of $2a = 14$ mm was used. It was driven with a constant amplitude of vibration velocity $v_m = 5$ cm/s within the range of measuring frequencies. The piston thickness was $b = 0.5$ cm.

For steel $E = 2 \times 10^{11}$ N/m^2, $\varrho = 0.78$ kg/m^2, $\nu = 0.27$. In the system under consideration the boundary conditions are not distinctly determined. However, it will be assumed that the best approximation to the boundary conditions are those corresponding to the supported plate. With this assumption and with data of the piston given above, from (4) we obtain the fundamental

eigenmode frequency $f_{01} = 1100$ Hz. The condition $ka = 1$ for the piston under consideration corresponds to a frequency of 775 Hz.

The piston was placed in a square baffle of side length $l = 2$ m and thickness 0.5 cm. The baffle was made from plywood and was clamped at the edges, by means of steel rods, to a structure which was not rigidly connected to the base of the drivers.

The lowest measuring frequency was established to be 200 Hz in order to fulfil the condition of the baffle dimensions $l > \lambda$.

With the above parameters of the system the calculated and measured results for both near and far field should agree within the frequency range from

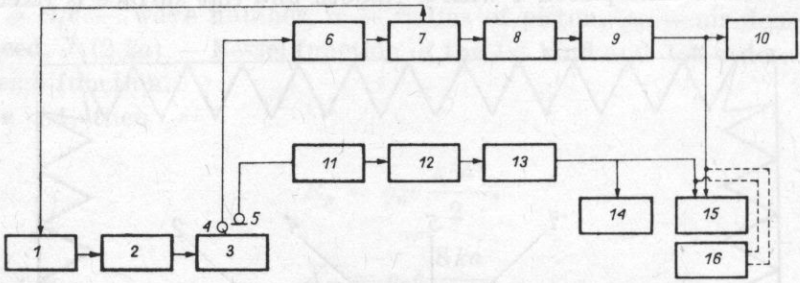

Fig. 2. Block diagram of the measurement system

1 – generator BK 1026, *2* – power amplifier BK 2707, *3* – measuring arrangement shown in Fig. 1, *4* – acceleration pick-up BK 4343, *5* – microphone BK 4138, *6* – amplifier BK 2626, *7* – integrating system BK 2625, *8* – microphone amplifier BK 2603, *9* – band-pass filter BK 1614, *10* – sound lever meter BK 2203, *11* – preamplifier BK 2619, *12* – microphone amplifier BK 2603, *13* – band-pass filter BK 1614, *14* – vibration meter BK 2510, *15* – phase shift meter BK 2911, *16* – analogue correlator DISA TCA system

200 to 775 Hz. In order to quantitatively verify the discrepancies at higher frequencies the measuring range was extended up to 2000 Hz.

The measurements were made by means of a 1/8″ microphone, type BK 4138, placed at a distance of 0.5 cm from the piston surface. In order to check the discrepancies in the results, produced by reflections between the microphone and the piston surface, measurements were performed for two positions of the microphone (Fig. 1), namely: perpendicular (a) and parallel, (b) to the piston surface. The piston velocity was measured by means of an accelerometer pick-up, type BK 4443, in conjunction with an integrating unit, type BK 2625.

Signals were transmitted from the microphone and pick-up to r.m.s. meters through two measuring channels (Fig. 2). The power level was determined in dB referred to a power of $W_0 = 10^{-12}$ W:

$$L_{pv} = 10 \log \frac{p_{aef} v_{ef} \pi a^2 \cos \varphi_{pvt}}{W_0} \text{ [dB]}. \tag{19}$$

The sound power of the piston was determined by employing two methods:

(a) a phase method using a phase meter BK 2971,

(b) a correlation method using a DISA correlator, type 55D70, in accordance with the block diagram shown in Fig. 2.

During preliminary testing, the effect of the following factors that would cause possible disagreement between the measured and calculated results was considered:

— a non-uniform distribution of vibration velocity over the piston surface,
— the position of the microphone,
— the phase shifts in different measuring channels.

The non-uniformity of the distribution of vibration velocity over the piston surface was examined by changing the position of the vibration pick-up on the piston surface. The maximum deviation ΔL of the velocity level and the change of the phase shift $\Delta\varphi_v$, with respect to the values obtained with the pick-up positioned at the centre of the plate, were measured. At a frequency of 1000 Hz, the results were $\Delta L = 1$ dB, $\Delta\varphi_v = 2^0$, while at 2000 Hz, $\Delta L = 3$ dB, $\Delta\varphi_v = 7^0$. Thus, in accordance with the calculations, the distribution of vibration on the piston surface can be assumed to be constant below 1100 Hz. For higher frequencies the non-uniformity of the velocity distribution must be taken into account.

Table 1 gives the results obtained for the 1/8″ microphone arranged perpendicularly and parallelly to the piston surface. The results indicate that there

Table 1. Differences in the sound power levels ΔL and in the phase shift angles $\Delta\varphi_p$ at two different microphone positions

f[Hz]	200	400	600	800	1000	1200	1600
ΔL[dB] $= L_\perp - L_\parallel$	0.5	0.5	0.5	0.5	0.0	−1.0	−1.5
$\Delta\varphi_p^\circ = \varphi_{p\perp}^\circ - \varphi_{p\parallel}^\circ$	−2	−1	−2	−3	−6	−4	−6

exists a small difference of levels, $\Delta L = L_\perp - L_\parallel$, and phase shifts, $\Delta\varphi_p = \varphi_{p\perp} - -\varphi_{p\parallel}$, for frequencies below 1000 Hz with a tendency for them to grow at higher frequencies.

The measured values of phase shift must be corrected due to the additional phase shifts (dependent on frequency) introduced by the measurement channels.

Denoting by φ_0 the phase shift value indicated by the phase meter, we can write the real value of phase shift between the sound pressure and the piston velocity as

$$\varphi_{pv} = \varphi_0 + \Delta\varphi, \tag{20}$$

where $\Delta\varphi$ is the error in the phase shift introduced by the experimental arrangement.

In the measuring arrangement used in these experiments the errors $\Delta\varphi$ consist of the following components: φ_p — from the amplifiers of the sound pressure measuring channel, φ_v — from the amplifiers of the velocity measuring

channel, φ_m — from the microphone, and $\varphi_{p\tau}$ — from the delay of acoustic pressure as a result of the distance r between the microphone and the piston surface

$$\varphi_{p\tau} = \frac{\omega r}{c} \times 360°. \tag{21}$$

Taking into account the signs of the phase shifts, we obtain

$$\Delta\varphi = \varphi_p - \varphi_v - \varphi_{pm} + \varphi_{p\tau}. \tag{22}$$

The calculated and measured values of phase shifts for the measuring frequencies are presented in Table 2.

Table 2. Results of measurements and calculations of phase shifts

f[Hz]	200	400	600	800	1000	1200	1600	2000
$\varphi_p^\circ - \varphi_v^\circ$	12	0	20	6	1	3	6	2
φ_{pm}°	0	0	0	0.5	1.5	2	3	5
$\varphi_{p\tau}^\circ$	1.2	2.1	3.1	4.2	5.2	6.2	8.3	10.4
$\Delta\varphi^\circ$	10.8	−2.1	16.9	2.3	−2.7	−1.2	0.7	−3.4
φ_0°	70	76	46	57	55	36	32	22
φ_{pv}°	80.8	73.9	62.9	59.3	52.3	34.8	32.7	18.6
φ_τ°	80	69	62	66	59	40	33	19
φ_{pvt}° (calculated)	81.5	74	65	59.5				
				57.5	48	45	36.5	31

4. The results of measurements and calculations of acoustic power under near field conditions

(a) *The phase method.* The sound power level of the piston was determined on the basis of the following measurements: the r.m.s. value of acoustic pressure p_{aef}, the r.m.s. value of velocity of the piston v_{ef} and phase shift φ_{pv}.

The results of the measurement of phase shifts as a function of frequency are presented in Fig. 3. The curve φ_0 represents the measured values without correction, φ_{pv} — with the correction according to (20), (21) and (22), φ_{pvt} — the values calculated from (13) for frequencies below 775 Hz and from (16) — above this value.

The measurements of the sound power level obtained by the phase method on the basis of (19) are presented in curve L_{pv} of Fig. 4. The curve L_t in Fig. 4 shows the values calculated from (17) for frequencies below 775 Hz, and from (18) above this value.

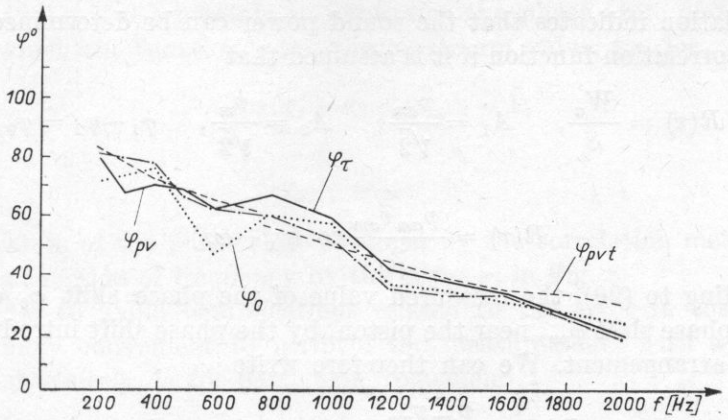

Fig. 3. Results of measurements and calculations of phase shifts φ as a function of frequency using: φ_{pv} – phase method with phase shift correction, φ_0 – the phase method without corrections, φ_τ – the correlation method, φ_{pvt} – theoretical calculations

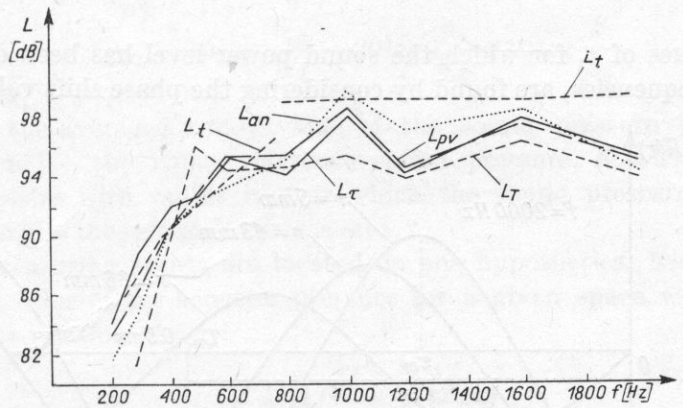

Fig. 4. Results of measurements and calculations of the sound power level of the piston as a function of frequency using: L_{pv} – the phase method, L_τ – the correlation method, L_{an} – the free field method ISO, L_T – the reverberation method, L_t – theoretical calculations on the basis of approximate formulae

(b) *The correlation method.* The cross-correlation function of two sinusoidal processes with amplitudes A_1 and A_2 and initial phases φ_1 and φ_2 takes the form

$$R(\tau) = \lim_{T\to\infty} \frac{1}{T} \int_{-T}^{T} A_1 \sin(\omega t + \varphi_1) A_2 \sin(\omega_t + \varphi_2 + \omega\tau)\, d\tau,$$

which, after being integrated, is simplified to the form

$$R(\tau) = A_1 A_2 \cos(\varphi_1 - \varphi_2 - \omega\tau). \tag{24}$$

This relation indicates that the sound power can be determined by means of a cross-correlation function if it is assumed that

$$R(\tau) = \frac{W_a}{S}, \quad A_1 = \frac{p_{am}}{\sqrt{2}}, \quad A_2 = \frac{v_m}{\sqrt{2}}, \quad \varphi_1 - \varphi_2 = \varphi_0, \tag{25}$$

and then

$$R(\tau) = \frac{p_{am} v_{am}}{2} \cos(\varphi_0 - \omega\tau). \tag{26}$$

According to (20), the measured value of the phase shift φ_0 differs from the actual phase shift φ_{pv}, near the piston, by the phase shift introduced by the measuring arrangement. We can therefore write

$$R(\tau) = \frac{p_{am} v_{am}}{2} \cos(\varphi_{pv} + \Delta\varphi - \omega\tau). \tag{27}$$

Hence, the radiated power described by equation (8) is determined if the condition

$$\omega\tau = \Delta\varphi \tag{28}$$

is satisfied.

The values of τ, for which the sound power level has been determined at particular frequencies, are found by considering the phase shift values presented

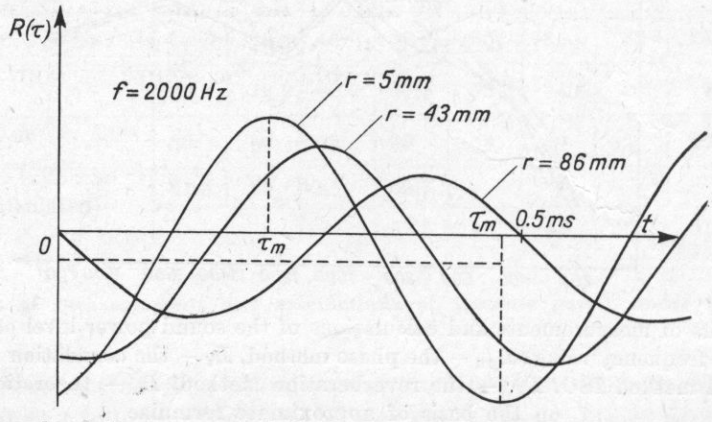

Fig. 5. An example of the cross-correlation curves used for the calculations of phase shift φ_τ and sound power level L_τ for different distances r between the microphone and the piston

in Table 2. Figure 5 represents a specimen of the correlation curves at 200 Hz for different distances r between the piston and the microphone. The sound power level obtained by the correlation method was calculated from the expression

$$L_\tau = 10 \log \frac{R(\tau) S}{W_0}, \tag{29}$$

and presented as the curve L_τ in Fig. 4.

From (27) it is also possible to determine the phase shift φ_τ for the value of τ_m for which the function takes the maximum value, i.e. for

$$\cos(\varphi_\tau + \Delta\varphi - \omega\tau_m) = 1, \tag{30}$$

hence

$$\varphi_\tau = \omega\tau_m - \Delta\varphi. \tag{31}$$

The values of the phase shift obtained by the correlation method are presented as a function of frequency by the curve φ_τ in Fig. 3.

In order to avoid complications related to the error in the phase shift $\Delta\varphi$, it is more convenient to perform the measurements with a phase shiftmeter which cancels $\Delta\varphi$ for particular frequencies.

5. The results of measuring acoustic power under far field conditions

(a) *Free field conditions method.* According to the ISO recommendations, the acoustic power level of a source is calculated from

$$L_{\text{ISO}} = 10\log\frac{W_a}{W_0} = 20\log\frac{p_a}{p_{a0}} + 10\log\frac{S}{S_0}, \tag{32}$$

where p_a is the averaged r.m.s. value of the sound pressure $[N/m^2]$, $p_{a0} = 2\times10^{-5}[N/m^2]$ – the r.m.s. reference sound pressure, $S = 2\pi r^2$ – the area of a hemisphere with radius r, over which the sound pressure is measured, and $S_0 = 1\ \text{m}^2$ – the reference surface area.

If all measuring points are located on one hypothetical hemisphere, then the average value of the acoustic pressure for a given space would be determined by the relation

$$\frac{p_a}{p_{a0}} = \sqrt{\frac{1}{n}\sum_{i=1}^{n}\left(\frac{p_{ai}}{p_0}\right)^2}, \tag{33}$$

where p_{ai} is the value of the sound pressure at the i-th measuring point, i – the number of a measuring point in an anechoic room (there were six positions of the microphone at a distance of $r = 1$ m from the piston), and n – the number of measuring points.

The measurements of the sound power level of the source, after averaging the sound pressures in free field conditions, are presented by curve L_{an} in Fig. 4.

(b) *The reverberation method.* The level of the sound power of the source in the reverberation field is described by

$$L_T = 10\log\frac{W_a}{W_0} = 20\log\frac{p_a}{p_{a0}} - 10\log T + 10\log V - 14 \quad [\text{d}B], \tag{34}$$

where p_a is the averaged r.m.s. value of the sound pressure for a microphone placed in the far field, T – the reverberation time [s], V – the volume of the room [m^3].

The measurements were performed in a reverberation chamber with a volume of $V = 196$ m^3. The results of measurement of the reverberation time after installation of the equipment (from Fig. 1) are given in Table 3.

The measurement results of the sound power level of the piston obtained by the reverberation method are illustrated by curve L_T in Fig. 4.

Table 3. Characteristics of the reverberation time of the reverberation chamber as a function of frequency after the equipment has been placed in it

f[Hz]	200	400	600	800	1000	1200	1600	2000
T [s]	6.4	6.7	5.8	5.0	5.2	4.5	3.2	3.3

6. Discussion of the results

The comparison of the calculated and measured results of the sound power level of the piston obtained for near field conditions and for far field conditions shows that there is a very good agreement at low frequencies. However, for higher frequencies, this agreement become worse.

The disagreement for higher frequencies is due to two factors: non-uniformity of the distribution of the velocity on the piston surface, and non-uniformity of the directional characteristics of the sound pressure radiated by the piston.

The non-uniformity of the velocity distribution depends on the mechanical properties of the piston expressed by its eigenmode frequencies. If follows from theoretical considerations that the experimental results would be expected to be 3 to 5 dB smaller than those calculated for the fundamental eigenmode frequency.

The non-uniformity of the distribution of the sound pressure depends on the non-uniformity of the velocity distribution on the piston surface and on the value of ka. For $ka > 1$ the piston will exhibit directional properties, which will effect the non-uniformity of the distribution of the acoustic field in the far field and, therefore, thus cause an increase of measurement errors.

The experimental results confirm the above conclusions on the disagreement of the results at higher frequencies. Near the first eigenmode frequency of the piston, the values measured by different methods show the sound power level to be about 4 to 5 dB lower than the calculated values.

Moreover, for $ka > 1$ the dispersion of the results increased and, therefore, it was necessary to use a greater number of measuring points.

7. Conclusions

1. The near field method of measurement of the sound source power level is suitable for measuring the vibrating elements for the low frequency range.

The accuracy of the method becomes worse for the frequency range over the eigenmode frequencies of the elements under test, when the element has dimensions large compared to the wavelength.

2. At higher frequencies, it is necessary to average the measurements of the vibration velocity and sound pressure at several measuring points or to calculate an equivalent vibrating area.

3. The correlation method is a very simple way of measuring the level of the power of the sound source. However, it requires to take into account the phase shifts of the measuring arrangement.

4. It could be expected that the present work should enable the correlation method to be applied for measuring the sound power level generated by particular elements of machinery.

References

[1] Z. ENGEL, R. PANUSZKA, *The method of the evaluation of vibro-acoustical emmission of complex mechanical systems on example of the rotor-plate system of the chamber airless shotblasting machine* [in Polish], Archiwum Akustyki, **10**, 4, 345-356 (1975).

[2] L. FILIPCZYŃSKI, *The near field distribution on the axis of the vibrating plate* [in Polish], Archiwum Akustyki, **3**, 4, 339-346 (1968).

[3] G. HÜBNER, *Analysis of errors in measuring machine noise under free-field conditions*, JASA, **4**, 967-977 (1973).

[4] ISO, R. 495. *General requirements for the preparation of test codes for measuring the noise emitted by machines.*

[5] I. MALECKI, *Physical fundamentals of technical acoustics*, Pergamon Press (1969).

[6] P. MORSE, *Vibration and sound*, McGraw-Hill, New York 1948.

[7] W. PAJEWSKI, *Radiation impedance of ceramic piezoelectric transducers* [in Polish], Archiwum Akustyki, **3**, 4, 347-362 (1968).

[6] Z. ŻYSZKOWSKI, *Fundamentals of electroacoustics* [in Polish], PWT, Warszawa 1966.

Received 10th February 1976

ARCHIVES OF ACOUSTICS
1, 3, 215-230 (1976)

THE CHARACTERISTIC DIFFERENTIAL SPECTRUM OF A CONVENTIONAL SUBSTITUTE SIGNAL SOURCE IN MACHINERY TESTING

WOJCIECH CHOLEWA

Silesian Technical University (Gliwice)

The paper concerns the evaluation of the acoustic signal which carries information on the dynamics of the interaction of machine elements. A method is presented which can be used for the experimental testing of machine characteristics by periodic excitation of the machine. The essence of this method is a new evaluation of the signal in the form of characteristic differential spectra which are dependent on the dynamics of the interaction of elements of the object to be tested and independent of the position of the microphone.

1. Introduction

The testing of machines by acoustic methods may involve attestation, diagnostic and constructional tests. This paper does not deal with attestation tests, the main purpose of which is the evaluation of noise and vibrations in the light of ergonomic criteria. The purpose of constructional tests is to check the tested object for design correctness. The purpose of diagnostic tests is the appraisal of the condition of a tested object. In the tests described here evaluation of the design and condition is made indirectly by evaluation of the dynamics of the interaction of the elements of the tested object. The conclusions will be based on the statement that the acoustic effects and vibrations of the object depend on the dynamics of the interaction of elements. Constructional tests should include several machines while diagnostic tests should cover only a single machine.

It has been assumed that the object to be tested may be described by

$$(K \wedge ST \wedge WD), \tag{1}$$

where K is the design of the tested object determined by the geometrical, material and dynamic features of the construction [3]; it constitutes the input information of the production process whose result is the tested object; ST is the condition of the tested object and describes a set of evaluations of the correctness test of operation and degree of wear of the object; WD are the operating

conditions that describe a set of inputs and outputs of the tested object (e.g. speed, power).

The design is understood to be the result of the designing process, but not a direct description of the tested object. For instance, a geometrical constructional feature concerning the shaft determines a permissible deviation of the diameter or the tolerance of the execution of the construction of such products including, among others, the tested object. This feature does not describe the value of the diameter determined by measurement of the tested object. The statement that the tested object corresponds to its design is an assumption that requires verification, which will consists, in part, in checking that the measurement system is within the assumed tolerance field.

One of the basic methods of analysis used in acoustic methods of machinery testing is a frequency analysis of the signals. A *signal* here means the acoustic effect or vibrations of the tested object. Signal spectra are a direct result of experimental tests. A *signal spectrum* in this paper will be the distribution of, the signal power in consecutive frequency bands with constant relative width-determined for a certain frequency range. It has been assumed that the descri bed spectrum is a set of power levels in these bands,

$$W = \{w(f_j),\ j = j_p, \ldots, j_k\}, \tag{2}$$

where W denotes the spectrum as a set, w – the signal power level in the frequency band [dB], f_j – the mid-band frequency [Hz], j – the index (serial number) of the frequency band varying from j_p to j_k for bands of mid-frequencies from f_p to f_k.

We use a simplified notational form for the definition:

(2) $$W = \{w(j),\ j = j_p, \ldots, j_k\}. \tag{3}$$

The classification of the frequency range into bands of constant relative width and the establishment of indices for the frequency bands has been formulated in order to adopt a uniform system of notation.

It has been assumed that

– 1000 Hz is always the mid-range frequency;

– the index of the band with mid-frequency 1000 Hz equals zero, i.e.

$$\begin{aligned} f_j &= 1000\ \text{Hz} \rightarrow j = 0, \\ f_j &< 1000\ \text{Hz} \rightarrow j < 0, \\ f_j &> 1000\ \text{Hz} \rightarrow j > 0; \end{aligned} \tag{4}$$

– the number which determines the accepted classification into bands and indirectly determines the band width is the so-called *band spacing* x,

$$x = f_{j+1}/f_j.$$

From the above we obtain

$$f_j = 1000\, x^j\ [\text{Hz}]. \tag{6}$$

Experimental tests have been performed for various conditions of the tested object. A limitation has been accepted that the tested objects are machines for which a certain characteristic excitation frequency f_m can be defined. For example, one of characteristic excitation frequencies f_m for gear transmissions is the meshing frequency f_z,

$$f_m = f_z \frac{nz}{60} \text{ [Hz]}, \tag{7}$$

where n is the rotational speed of the toothed element [r.p.m.] and z — the number of teeth on the toothed element.

It has been assumed that the characteristic frequency f_m is equal to the mid-band frequency of one of the bands with fixed relative width. This obviously limits the operating conditions which may be established during testing. For instance, if the tested object is a gear transmission, then the rotational speed can be evaluated from the following formula:

$$n_j = 60\,000\, x^j/z \text{[r.p.m.]} \quad \text{for } j = 0, \pm 1, \pm 2, \ldots \tag{8}$$

The index m, in the denotation of the characteristic frequency f_m, is an integer equal to the index j of mid-band frequency f_j equal to f_m. Thus from equation (6)

$$m = \log_x(f_m/1000). \tag{9}$$

2. Spectra of the characteristic and resonance signals

The spectra of signals determined for various operating conditions of a large number of gear transmissions [1, 4, 6] have been compared. Special attention was paid to the occurrence of local maxima of the spectrum caused by resonance phenomena, as well as to the occurrence of maxima that correspond to the harmonics and subharmonics of the meshing frequencies. It has been found [1] that, for a limited range of operating conditions, the signal spectrum can be regarded as the sum of the spectra of three independent signals,

$$W = S + R + L, \tag{10}$$

where W is the spectrum of the analyzed signal, S — the spectrum of a signal called the characteristic signals, R — the spectrum of a signal called the resonance signal, and L — the spectrum of a signal referred to as pink noise.

The characteristic signal depends on the dynamics of the interaction of the elements of the tested object and on the value of the characteristic frequency f_m determined by the design and operating conditions of the object.

A feature of this signal is the stability of its spectrum described on a relative scale of frequency, that is on a frequency scale referred to the characteristic frequency f_m (Fig. 1).

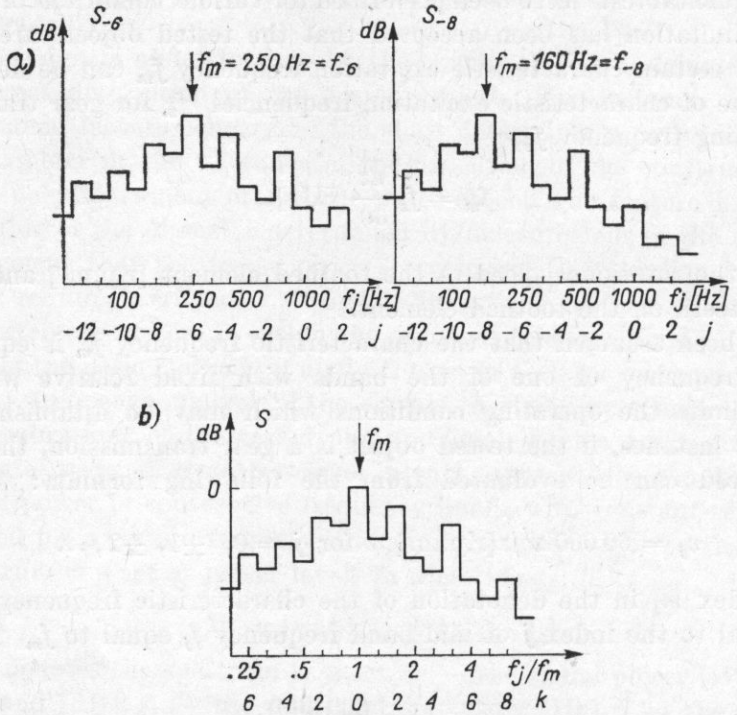

Fig. 1. Characteristic spectrum: a) in terms of an absolute frequency scale for various characteristic frequencies, b) in terms of a relative frequency scale

The spectrum of the characteristic signal can be written:

— in terms of an absolute scale of frequency as

$$S_m = \{s_m(j),\ j = j_p, \ldots, j_k\}, \tag{11}$$

where $s_m(j)$ is the value of the power level of a typical signal in the j-th frequency band for a characteristic frequency equal to f_m;

— and in terms of relative scale of frequency as

$$S = \{s(k),\ k = k_p, \ldots, k_k\}, \tag{12}$$

where

$$s(k) = s_m(k+m). \tag{13}$$

The resonance signal does not depend on the operating conditions of the tested object. Its spectrum describes the resonance properties of the object and can be denoted as

$$R = \{r(j),\ j = j_p, \ldots, j_k\}. \tag{14}$$

In view of the necessity to establish reference levels for characteristic and resonance signals it has been assumed that:

– the level of the spectrum of the typical signal $s(k)$ for the mid-band frequency $f_j = f_m$ is equal to 0 dB,

$$s(0) = 0\,[\mathrm{dB}], \tag{15}$$

– and the level of the resonance signal spectrum for the mid-band frequency of 1000 Hz is equal to 0 dB,

$$r(0) = 0\,[\mathrm{dB}]. \tag{16}$$

Bearing in mind the assumptions (15) and (16) and the dependence (10), a third signal in the form of pink noise has been introduced. The spectrum of this signal is described by a constant level l_m of the power in all frequency bands. It can be interpreted as the power $w(j)$ of the analyzed signal in the mid-frequency band (at 1000 Hz) for operating conditions that cause the occurrence of a characteristic frequency $f_m = 1000$ Hz.

Within the range of the tests performed on gear transmissions [1], a relationship between the tested object, the measuring conditions and the spectra defined (S, R, L), was found to exist (Fig. 2).

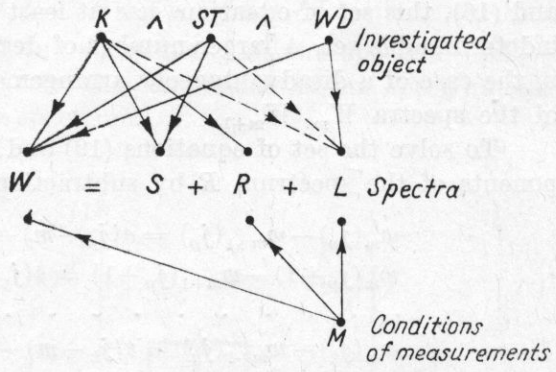

Fig. 2. Relationships encountered between the tested object, the measuring conditions and the defined spectra S,R,L

For the calculation of the spectra S, R and L, it is necessary to measure spectra for various operating conditions, i.e. for various characteristic frequencies. The number of different characteristic frequencies for which spectra W are determined should be at least 2. If the number is greater than 2, it is possible to calculate the spectra to be determined and to define the confidence interval for their components.

3. Determination of the spectra S, R and L-differential spectra

The results of measurements made are spectra W_m determined in the range $f_p - f_k$ at characteristic excitation frequencies f_m equal to successive mid-band frequencies m, $m+1$, ...

Let the number of f_m be equal to 2. On the basis of equation (10) we can write

$$W_m = S_m + R + L_m \tag{17}$$

and

$$W_{m+1} = S_{m+1} + R + L_{m+1}. \tag{18}$$

In equations (17) and (18) the unknowns are S_m, S_{m+1}, R, L_m and L_{m+1}. Using (13) we can write equations (17), (18) in the form:

$$\begin{aligned} w_m(j_p) &= s(j_p - m) + r(j_p) + l_m, \\ w_m(j_p+1) &= s(j_p+1-m) + r(j_p+1) + l_m, \\ &\cdots\cdots\cdots\cdots \\ w_m(j_k) &= s(j_k - m) + r(j_k) + l_m; \end{aligned} \tag{19}$$

$$\begin{aligned} w_{m+1}(j_p) &= s\big(j_p - (m+1)\big) + r(j_p) + l_{m+1}, \\ w_{m+1}(j_p+1) &= s\big(j_p+1-(m+1)\big) + r(j_p+1) + l_{m+1}, \\ &\cdots\cdots\cdots\cdots \\ w_{m+1}(j_k) &= s\big(j_k - (m+1)\big) + r(j_k) + l_{m+1}. \end{aligned} \tag{20}$$

It can be proved that after giving consideration to the conditions (15) and (16), this set of equations has at least one degree of freedom, i.e. it is an indeterminable set. A larger number of degrees of freedom can be encountered in the case of a disadvantageous arrangement of the values of the components of the spectra W_m, W_{m+1}.

To solve the set of equations (19) and (20), we remove the unknown components of the spectrum R by subtraction of corresponding equations

$$\begin{aligned} w_m(j_p) - w_{m+1}(j_p) &= s(j_p - m) - s(j_p - m - 1) + d, \\ w_m(j_p+1) - w_{m+1}(j_p+1) &= s(j_p+1-m) - s(j_p - m) + d, \\ &\cdots\cdots\cdots\cdots \\ w_m(j_k) - w_{m+1}(j_k) &= s(j_k - m) - s(j_k - m - 1) + d, \end{aligned} \tag{21}$$

where

$$d = l_m - l_{m+1}. \tag{22}$$

Substituting from (15) into (21) we get

$$\begin{aligned} w_m(m) - w_{m+1}(m) &= 0 - s(-1) + d, \\ w_m(m+1) - w_{m+1}(m+1) &= s(1) - 0 + d. \end{aligned} \tag{23}$$

Thus the solution of the equation set (21) may be obtained in the form of a family of solutions, with family parameter equal to d.

The form of the solutions is

$$S = \{s(k),\ k = j_p - m - 1, \ldots, j_k - m\}, \tag{24}$$

where $s(k)$ is defined by the recurrence relations

$$s(k) = s(k-1) + w_m(m+k) - w_{m+1}(m+k) - d, \tag{25}$$

and

$$s(k) = s(k+1) + w_{m+1}(m+k+1) - w_m(m+k+1) + d. \tag{26}$$

Proceeding in a similar manner it is possible to determine the spectrum R.

The concept of differential spectra ΔS and ΔR, defined as invariants of the family of solutions of the set of equations (21) may be introduced. For the form of these spectra we have

$$\Delta S = \{\Delta s(k), \quad k = j_p - m, \ldots, \quad j_k - m - 1\}, \tag{27}$$

$$\Delta R = \{\Delta r(j), \quad j = j_p + 1, \ldots, \quad j_k - 1\}, \tag{28}$$

where

$$\Delta s(k) = s(k) - \tfrac{1}{2}[s(k-1) + s(k+1)], \tag{29}$$

$$\Delta r(j) = r(j) - \tfrac{1}{2}[r(j-1) + r(j+1)]. \tag{30}$$

Substituting from (25) and (26) into (29) we obtain:

$$\Delta s(k) = \tfrac{1}{2}[w_m(m+k) - w_m(m+k+1) + w_{m+1}(m+k+1) - w_{m+1}(m+k)]. \tag{31}$$

Similarly:

$$\Delta r(j) = \tfrac{1}{2}[w_m(j) + w_{m+1}(j) - w_m(j-1) - w_{m+1}(j+1)]. \tag{32}$$

The graphical representation of the components of the spectrum ΔR is shown in Fig. 3. It should be stressed that the components of this spectrum are very sensitive to local extremes of the spectrum.

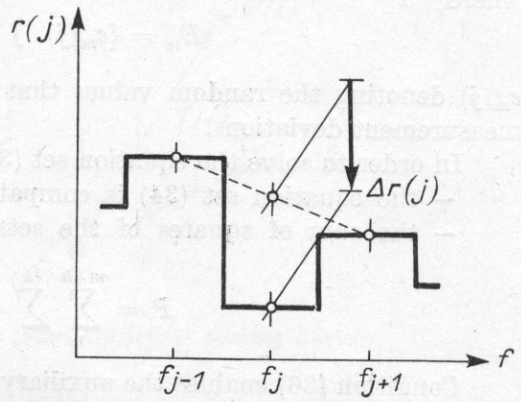

Fig. 3. Component $\Delta r(j)$ of a differential resonance spectrum

4. Deviation of differential spectra

The above method of determining the spectra ΔS, ΔR on the basis of knowledge of the spectra W_m, W_{m+1} does not permit the determination of the deviations and confidence interval for components of the spectra ΔS, ΔR that are looked for.

To determine the deviations of the spectra of interest, it is necessary to know the set of spectra $W_m, W_{m+1}, \ldots, W_{m+h}$, where h is higher than unity.

The determination of the spectra ΔS and ΔR now involves solving the following equations:

$$\begin{aligned} W_m &= S_m + R + L_m, \\ W_{m+1} &= S_{m+1} + R + L_{m+1}, \\ &\cdots\cdots\cdots\cdots \\ W_{m+h} &= S_{m+h} + R + L_{m+h}. \end{aligned} \tag{33}$$

Attention should be called to the fact that the spectra $W_m, W_{m+1}, \ldots$, are determined by measurement and as such involve a certain deviation due to the measurement itself. These deviations cause the spectra ΔS, ΔR, determined according to equations (31) and (32), from successive pairs of equations of (33), to be different and thus to cause a variance in this equation system. An additional reason for the variance of the equation set (33) may be ascribed to the fact that the assumptions on which it is based have not been fully satisfied.

To obtain the most reliable solution ΔS, ΔR, the so-called «agreement» of the equation set (33) is found in the form

$$\begin{aligned} W_m + E_m &= S_m + R + L_m, \\ &\cdots\cdots\cdots\cdots \\ W_{m+h} + E_{m+h} &= S_{m+h} R + L_{m+h}, \end{aligned} \tag{34}$$

where

$$E_m = \{e_m(j),\ j = j_p, \ldots, j_k\}, \tag{35}$$

$e_m(j)$ denoting the random values that indicate the existence of some slight measurement deviations.

In order to solve the equation set (34), two conditions are assumed:

— the equation set (34) is compatible;

— the sum of squares of the sets $E_m, E_{m+1}, \ldots$, is the least possible:

$$P = \sum_{i=m}^{m+h} \sum_{j=j_p}^{j_k} e_i^2(j) \Rightarrow \min. \tag{36}$$

Condition (36) enables the auxiliary unknowns e_i to be removed and makes it possible to form the equation set (34) into a compatible set of linear equations with regard to S, R and L. The equation set obtained in this manner has, like the set (19) and (20), at least one degree of freedom. The solution can be determined in the form of invariants of a family of solutions, that is, in the form of differential spectra ΔS, ΔR. This procedure permits the definition of deviations of the determined magnitudes of ΔS and ΔR. A disadvantage of this method is the necessity to solve very large sets of linear equations.

To avoid this problem, the following method for the determination of the solution of equation set (33) may be used:

– to divide the given spectra W into pairs of successive spectra $(W_m, W_{m+1})_1 (W_{m+1}, W_{m+2})_2, \ldots$;

– to determine for each pair according to (31), (32) the solution $(\Delta S, \Delta R)_1 (\Delta S, \Delta R)_2, \ldots$, which should be interpreted as approximate solutions;

– to accept the mean approximate solution as a solution of the set (33);

– and to determine the deviation of the solution obtained by comparing it with the approximate solutions.

5. Substitute signal source

The method described above for the evaluation of acoustic signals, is convenient for tests performed in laboratory conditions with negligible participation of the background. Full advantage is taken of the measurement results obtained for one location of the sensing device.

As it is necessary to conduct investigations in industrial conditions, a model of the system: object-sensing device (Fig. 4) has been used, and the notion of a substitute source introduced.

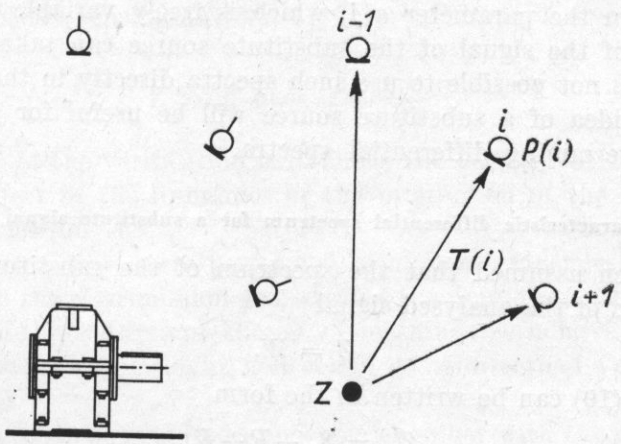

Fig. 4. Model of the system : tested object – sensing devices

The substitute source is a conventional source. For an established measuring point system it replaces the tested object. According to the accepted model for each measuring point i we may write

$$P(i) = Z - T(i), \tag{37}$$

where $P(i)$ is the spectrum of the signal at the measuring point i,

$$P(i) = \{p(i, j), j = j_p, \ldots, j_k\}, \tag{38}$$

Z — the spectrum of the substitute signal source,

$$Z = \{z(j), j = j_p, \ldots, j_k\}, \tag{39}$$

and $T(i)$ — the attenuation spectrum between the substitute source and the measuring point i,

$$T(i) = \{t(i, j), j = j_p, \ldots, j_k\}. \tag{40}$$

For any frequency band j, as well as for successive measuring points i, it is possible to write equation (37) in the form

$$\begin{aligned} z(j) - t(i_p, j) &= p(i_p, j), \\ z(j) - t(i_p + 1, j) &= p(i_p + 1, j), \\ &\cdots \\ z(j) - t(i_k, j) &= p(i_k, j), \end{aligned} \tag{41}$$

where $I = \{i_p, i_{p+1}, \ldots, i_k\}$ denotes a set of indices for the measuring points.

The solution of the equation set (41) can be represented in the form of a family of solutions with one parameter $a(j)$

$$z(j) = [z^*(j) + a(j)], \quad t(i, j) = [t^*(i, j) + a(j)], \tag{42}$$

where $z^*(j), t^*(i, j)$ is any pair of solutions satisfying the set (41).

From formulae (42) it can be seen that since the solution of the set (41) is dependent on the parameter $a(j)$ which is freely variable with frequency, the spectrum of the signal of the substitute source can take any form. For this reason it is not possible to use such spectra directly in the investigations. However, the idea of a substitute source will be useful for generalizing the method of determining differential spectra.

6. Characteristic differential spectrum for a substitute signal source

It has been assumed that the spectrum of the substitute signal source is the spectrum of the analysed signal

$$Z = W. \tag{43}$$

Equation (10) can be written in the form

$$Z_m = S_m + R + L_m, \tag{44}$$

where, from (37),

$$Z_m = P_m(i) + T(i). \tag{45}$$

The index m is defined by formula (6).

The concept of a resonance spectrum $R(i)$ can be introduced. For a measuring point i it is defined as

$$R(i) = R - T(i), \tag{46}$$

where

$$R(i) = \{r(i, j), j = j_p, \ldots, j_k\}, \tag{47}$$

$$r(i, j) = r(j) - t(i, j). \tag{48}$$

A similar dependence can be written for several measuring points $i, i+1, \ldots$ Hence we obtain:

$$\begin{aligned} P_m(i) &= S_m + R(i) + L_m, \\ P_{m+1}(i) &= S_{m+1} + R(i) + L_{m+1}, \\ &\cdots\cdots\cdots\cdots \\ P_m(i+1) &= S_m + R(i+1) + L_m, \\ P_{m+1}(i+1) &= S_{m+1} + R(i+1) + L_{m+1}. \\ &\cdots\cdots\cdots\cdots \end{aligned} \tag{49}$$

These equations can be solved in a similar manner to equations (33), i.e. by averaging successive approximated solutions. Accordingly, we obtain differential spectra ΔS, $\Delta R\,(i)$. The spectrum ΔS is the characteristic differential spectrum for the substitute signal source. The spectrum $\Delta R(i)$ is the differential spectrum of the resonance spectrum determined for the i-th measuring point.

According to the assumptions introduced, the spectrum ΔS is conditioned by the dynamics of the interaction of elements of the tested object. The analysis of this spectrum can be very effective in the diagnostic and constructional testing of machines. It should be stressed that the spectrum ΔS is not dependent on the location of the sensing device.

7. Verification of method

The purpose of the verification is to check the validity of the assumption regarding the effect of the dynamics of the interaction of the elements upon the shape of spectrum ΔS.

The verification tests were performed using gear transmissions [1] as the tested objects. In the transmission gears tested the dynamics of the interactions involved in the of three different shapes of meshing teeth have been differentiated. Transmissions with straight, helical and straight teeth of a different height have been tested.

The tests were performed in an anechoic chamber with the aid of standard Brüel and Kjaer apparatus. The microphone was placed at three different measuring points. The operating conditions were such as to obtain at least three values of meshing frequency. The signal spectra were measured in third octave bands.

Figure 5 shows characteristic differential spectra of the substitute signal source calculated for the three different shapes of teeth that determine the different dynamics of intermeshing. In Fig. 5 the broken line indicates the confidence intervals of component levels of the spectrum. These intervals are calculated by assuming a significance level of 0.9. Comparing the spectra shown, and taking into consideration their confidence intervals, it can be demonstrated [1] that

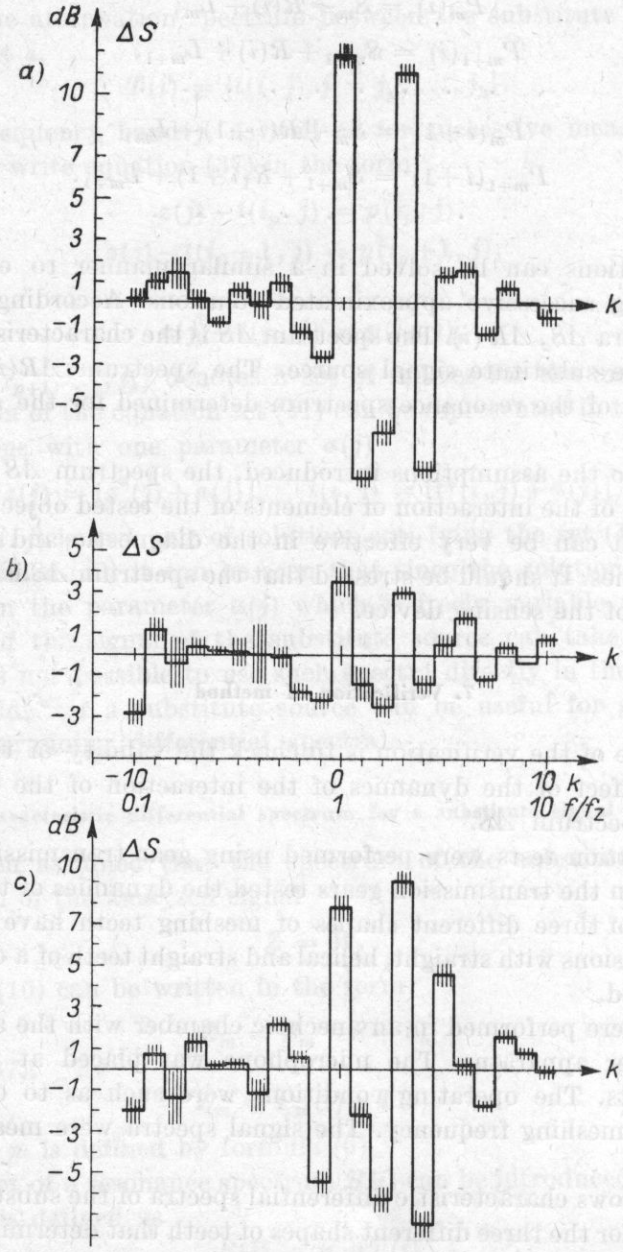

Fig. 5. Typical differential spectra for transmission gears of differently shaped teeth
a) straight teeth, b) helical teeth, c) straight teeth of a different height

they have essential differences. The conclusion can be drawn that different shapes of the spectrum ΔS correspond to different dynamics of intermeshing.

8. An example of the method application

The possibility of using the above method may be shown by an example. The tested object will be a single-stage transmission gear. The number of teeth of the pinion is $z_1 = 32$, and of the wheel $z_2 = 49$. The condition of the transmission is unknown. The possibility of performing the tests in laboratory conditions with the background being neglected, will be assumed.

The purpose of the investigation is the evaluation of the condition of the transmission gear in operating conditions that limit the pinion speed from 1000 to 1500 r.p.m. To determine the spectra a third octave analyser was used, with the microphone in a fixed position. Accoording to formula (5) for third octave bands

$$x = \sqrt[10]{10} = 1.2589.$$

The speed of the pinion in the transmission gear required during testing can be evaluated from formula (8). For the condition $1000 \leqslant n \leqslant 1500$ r.p.m. the following values have been calculated:

$$n_{-2} = 60000 \times 1.2589^{-2}/32 = 1183 \text{ r.p.m.},$$

$$n_{-1} = 60000 \times 1.2589^{-1}/32 = 1489 \text{ r.p.m.}$$

According to formula (7) these speeds correspond to excitation frequencies

$$f_{-2} = \frac{1183 \times 32}{60} = 630.9 \text{ Hz},$$

and

$$f_{-1} = \frac{1489 \times 32}{60} = 794.3 \text{ Hz}.$$

Investigation of the acoustic effect was carried out for the calculated rotational speeds. The microphone was provided at a measuring point located over the contract area at a distance of 1 m from the transmission gear box. The signal spectra obtained shown in Fig. 6. Typical differential spectra have been calculated according to formula (31) and are shown in Fig. 7.

Analysis the spectrum ΔS reveals maxima for frequencies f_z, 4 f_z, 0.25 f_z, 0.0315 f_z, 0.02 f_z. The frequency f_z is the meshing frequency. The frequencies 0.0315 f_z and 0.02 f_z correspond to the frequencies of the pinion and the wheel f_{01}, f_{02} calculated from the formulae

$$f_{01} = \frac{n}{60}, \quad f_{02} = \frac{nz_1}{60\, z_2}. \tag{50}$$

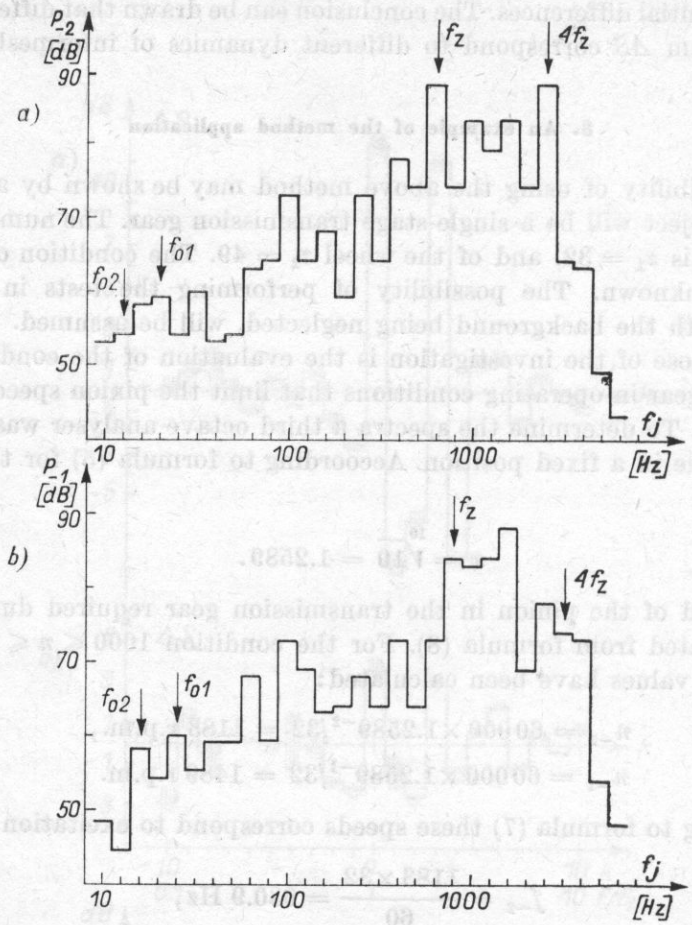

Fig. 6. Measurements of the spectra of the acoustic signal from a transmission gear; a) $n = 1183$ r.p.m., b) 1489 r.p.m.

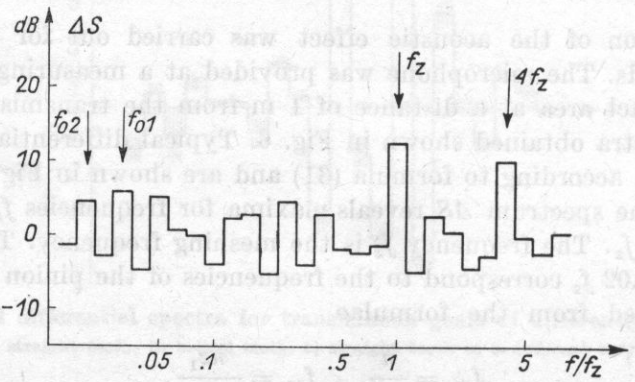

Fig. 7. Calculated characteristic differential spectrum for a transmission gear

On the basis of investigations of transmission gears over many years, it can be said, in virtue of the occurrence in a spectrum of local maxima at relevant frequencies, that it is possible to determine the probable condition of the tested object in accordance with the following data:

f_z — nonlinear entering of teeth into contact causes an excessive dynamic in the intermeshing,

$4f_z$ — eccentricity of the base circle of cut teeth,

$0.25f_z$ — unevenness of execution deviations on the circumference of the toothed element,

$f_{01} = 0.0315f_z$ — no balancing of the pinion,

$f_{02} = 0.02f_z$ — no balancing of the wheel.

The description of the maxima occurring on the basis of the measurement results alone (Fig. 6) is not explicit, and alone they cannot provide the above conclusions.

It should be stressed that in practice it is necessary to measure the spectra in bands narrower than third octave bands. The method described imposes no limitations in this respect.

9. Conclusions

The method described for evaluating a signal in the form of typical differential spectra can be used in constructional and diagnostic tests of machine characteristics for some periodic excitation.

The typical spectrum introduced is independent of the position of the microphone or the vibration sensing device. This independence is of great importance in drawing conclusions about the state of the tested object.

The method proposed can be used with advantage when introducing automation of the measuring system and results of the spectrum analysis are obtained in a form permitting the direct input of these results as data for calculation on a digital machine. This requires the use of a spectrum analyser with an output via a digital-analoque converter to the paper punch, or of a spectrum analyzer operating on-line with a digital machine, or a special analyzer with an analogue input which can rapidly perform Fourier transforms.

References

[1] W. CHOLEWA, *A method for the evaluation of the acoustic signal of transmission gears for constructional testing* [in Polish], Institute of Fundamental Design of Machines, issue 22/56, Gliwice 1974.

[2] W. CHOLEWA, W. MOCZULSKI, *An investigation into the analysis of signals during constructional tests; and cooperation with industry in this field* [in Polish], Institute of Fundamental Design of Machines, issue 21/55, p. 21-35, Gliwice 1974.

[3] J. DIETRYCH, *Designing and construction* [in Polish], WNT, Warszawa 1974.

[4] J. DIETRYCH, Z. JASKÓŁA, M. MAKOMASKI, *Frequency characteristics and correlation function in the evaluation of the construction and state of gear transmissions* [in Polish] KOPKM Silesian Technical University, issue 30, Gliwice 1969.

[5] Z. JASKÓŁA, *Acoustic analysis of the effect of constructional features of transmission gears* [in Polish], KOPKM Silesian Technical University, issue 21, Gliwice 1966.

[6] M. MAKOMASKI, *Investigation of the effects of constructional features of transmission gears upon propabilistic characteristics of acoustic effects* [in Polish], IMiPKM Silesian Technical University, issue 4/38, Gliwice 1972.

Received 4th February 1975

ARCHIVES OF ACOUSTICS
1, 3, 231-242 (1976)

A BÉKÉSY AUDIOMETER WITH ELECTRONIC SIGNAL LEVEL CONTROL AND ITS APPLICATION TO PSYCHOACOUSTICAL MEASUREMENTS

ANTONI JAROSZEWSKI, ANDRZEJ RAKOWSKI

Laboratory of Musical Acoustics, Academy of Music (Warszawa)

Improvements introduced in the new version of a Békésy automatic audiometer with electronic control of signal level are described, with some details of the separate circuits used.

Examples of the uses of the new audiometer in threshold audiometry and some other applications are discussed.

1. Introduction

Some years ago the concept of the realization of the Békésy audiometer with electronic control of the signal level was published [15]; the possibility of the realization of this concept using conventional generally available laboratory equipment being pointed out. The new audiometer thus developed was patented in Poland [16]. The simpler version of this concept was later given by MOHL [14]. The common feature of Békésy type audiometers is the possibility of the continuous tracking and recording of the threshold level, as a function of time (at a constant frequency) or as a function of frequency, which automatically changes with time at a predetermined constant rate. The subject's task is to keep the signal level near the threshold by operating a switch which, depending on the position, causes the continuous growth or decrease of the signal level.

With regard to typical commercially available automatic Békésy audiometers, and some unique laboratory-developed systems of that kind [4, 13], one of the basic advantages of the new audiometer is the elimination of electromechanical step attenuators. The signal level is controlled continuously, using electronic volume control circuits, rather than step by step as in previous constructions in which potentiometers or attenuators and servomotors were commonly used.

The new Békésy audiometer with electronic level control, which has been used and progressively improved for over 6 years in our laboratory is basically constructed with typical Brüel and Kjaer laboratory equipment.

The latest version of the audiometer is characterized by the following specification:

1. Frequency range (without threshold equalizer) 20 Hz-20 kHz.
2. Frequency range with threshold equalizer 40 Hz-12 kHz.
3. Time of frequency scanning over the range 20 Hz-20 kHz, 10 s – over 100 hrs.
4. Dynamic range of the record 10, 25, 50, 75 dB (depending on the recording potentiometer used).
5. Paper speed 0.003-100 mm/s.
6. Writing speed 2-1000 mm/s.
7. Signal level control rate 3, 10, 30, ..., 100 dB/s.

In the present report some representative results of measurements carried out using the improved version of the audiometer are given to illustrate its possible applications in the fields of psychoacoustics and clinical audiometry. The new units which have been constructed and introduced since the first version of the new audiometer was publis hed [15] aredescribed in some detail.

2. Threshold equalizer

As a rule isophonic threshold equalization is introduced in clinical audiometers now in use. In such audiometers, or specifically on the audiograms, the normal hearing in the 18 to 25 years age group is represented as a straight horizontal line. Deviation of the record below this line corresponds to hearing loss and, vice versa, deviation of the record above the normal hearing line corresponds to hearing better than the average.

In order to make the operation of the new audiometer as close to the requirements developed and well accepted over the years of clinical practice as possible, threshold equalization was introduced in the present version. This results in a simplified interpretation of the records obtained compared to those from the former version, as well as in some improvement in accuracy.

The frequency response of the threshold equalizer was assumed to be equivalent to the ZWICKER and FELDTKELLER data [17] with an accuracy of approximation ± 1 dB. Active elements were used in the network to simplify the computation and to avoid attenuation which is usually significant in passive networks. Active elements are also more easily available and much smaller, particularly in the low frequency range where inductances for the passive LCR networks reach from 5 to 10 H.

The preliminary modelling of the equalizer networks was performed using a digital computer*. The final adjustments of the frequency response were

* Computer programme in ALGOL-Archives, Lab. of Musical Acoustics.

done on the completed network using an analogue tracer and a step by step error elimination technique.

The assumed frequency response of the equalizer was obtained using three almost independent networks. Their outputs are added in the output amplifier supplying power to a 600 ohm load (6 V at 40 Hz). This load is the input im-

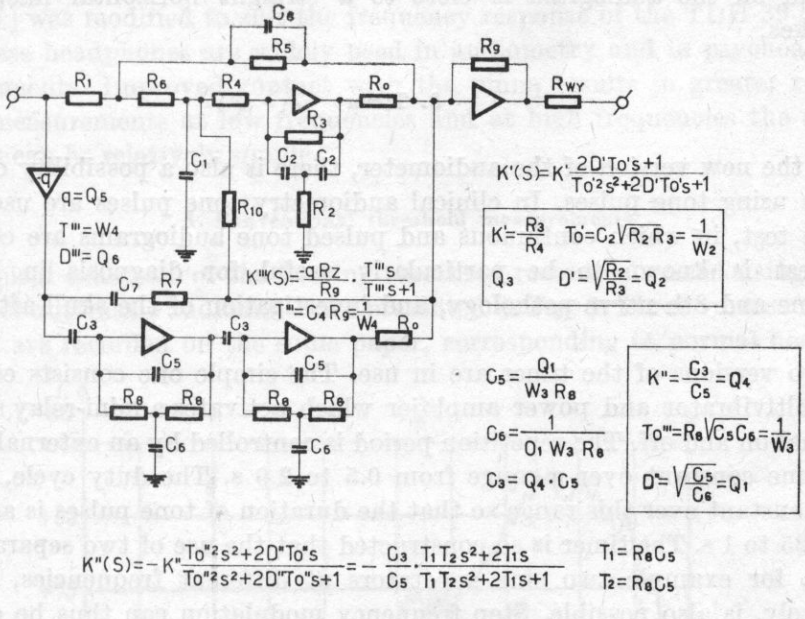

Fig. 1. Block diagram of the threshold equalizer according to Zwicker and Feldtkeller data [17] with symbols used in the computer programme

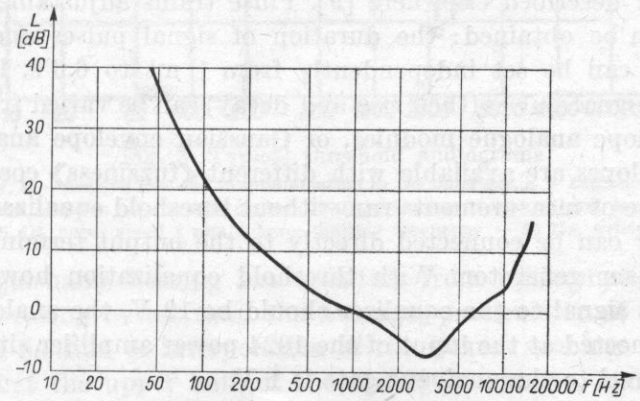

Fig. 2. Frequency response of the threshold equalizer

pedance of the modified version of the Beyer-DT-48 headphones equalizer described by ZWICKER and FELDTKELLER [17].

The low and high frequency networks consist essentially of operational amplifiers with «shunted T» filters in the feedback loops. The mid-frequency network, apart from passive elements contains an RC differential network and inverter to shape up the «drop» between the frequencies 2 and 5 kHz, Fig. 2.

With the two equalizers involved, the record of a normal hearing threshold on the audiogram is close to a straight horizontal line, halving the spikes.

3. Timer

In the new version of the audiometer, there is also a possibility of measurements using tone pulses. In clinical audiometry tone pulses are used in the Jerger's test, in which continuous and pulsed tone audiograms are compared. This test is known to be particularly useful for diagnosis in Menière's syndrome and 8th nerve pathology, and investigation of the skull after injury cases.

Two versions of the timer are in use. The simple one consists essentially of a multivibrator and power amplifier which activates a mini-relay switching the signal on and off. The repetition period is controlled by an externally adjustable time constant over a range from 0.5 to 2.0 s. The duty cycle, equal to 0.5, is constant over this range so that the duration of tone pulses is adjustable from 0.25 to 1 s. The timer is so constructed that the use of two separate signal sources, for example two sine generators at different frequencies, switched alternately, is also possible. Step frequency modulation can thus be obtained. A band pass filter is used to eliminate undesired transients.

The other version of the timer is based on the use of a multichannel analogue modulator described elsewhere [9]. Pulse trains adjustable within a wide range thus can be obtained: the duration of signal pulses and the intervals between them can be set independently from 1 ms to 6.6 s. In addition, the flanks of the signal pulses (their rise and decay) can be varied from 1 to 500 ms using linear slope analogue modules, or Gaussian envelope analogue modules. Gaussian envelopes are available with different «fuzziness» coefficients.

In the case of measurements run without threshold equalization, the analogue modulator can be connected directly to the output terminals of the 1024 Brüel and Kjaer generator. With threshold equalization however, in which case the input signal to the equalizer should be 12 V, the analogue modulator should be connected at the input of the 1024 power amplifier since the nominal input signal level to the analogue gate is 1 V.

Combining the Békésy audiometer with the analogue modulator is particularly convenient in measurements of simultaneous or post-stimulatory masking or pulsation threshold. Békésy tracing is very useful in these cases and results in a simplification of procedure and a significant decrease in the duration of the experiments [7].

4. Headphone equalizer

For some purely technical reasons the Telephonics TDH-39 headphones with MX 41 AR cushions were used in the present version of the audiometer, replacing the headphones used formerly, Beyer DT-48. Thus the previous headphone equalizer constructed according to ZWICKER and FELDTKELLER data [17] was modified to suit the frequency response of the TDH-39 headphones. These headphones are widely used in audiometry and in psychoacoustical measurements. Improved contact with the pinna results in greater reliability of the measurements at low frequencies and at high frequencies the equalizer network can be relatively simple.

5. Conventional threshold measurements

Typical examples of the hearing threshold records obtained using the new version of automatic audiometer are presented in Fig. 3. Three various threshold tracings are recorded on the same paper, corresponding to normal hearing (a),

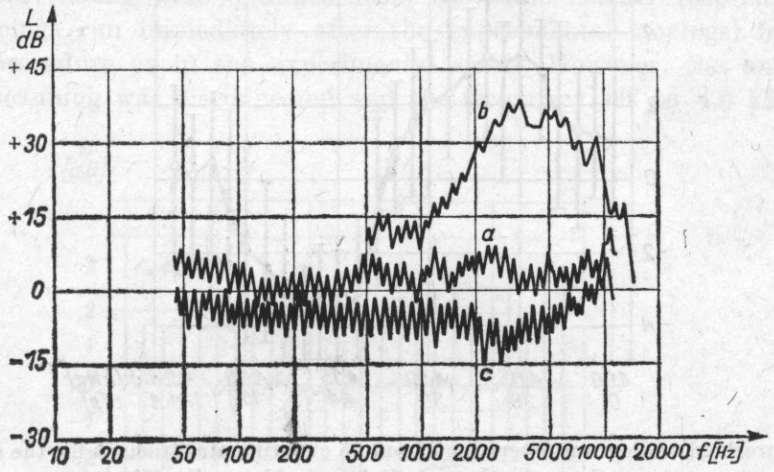

Fig. 3. Typical threshold audiograms

a – normal hearing, *b* – hearing loss due to inflammation in the inner ear, *c* – supranormal hearing between 2 and 3 kHz; tracings *a* and *c*: rate of level control 10 dB/s, tracing *b*: rate of level control 3 dB/s; recording potentiometer – 75 dB, paper speed 1 mm/s, lower limiting frequency – 50 Hz, writing speed – 100 mm/s

clearly distinguishable hearing loss resulting from inflammation in the inner ear (b), and hearing better than the average, particularly at mid-frequencies (c). The usual method of interpolation of the Békésy tracings is based on the assumption that the upper half of the spikes lies above, and the lower half below the threshold, the threshold usually being determined as a line halving the spikes (i.e. the mean value of the extremes). This assumption, however, does not seem to be fully acceptable and such an interpretation of Békésy tracings should be regarded as only approximate, particularly at higher rates of the signal level control.

It has to be pointed out that in the audiometer described, hearing loss or supranormal hearing are represented in the record or tracing by a deviation of the recording in a direction opposite to that in typical, clinical commercially available audiometers. To reverse the direction of the recording would require substantial redesigning of the 2305 level recorder, which in the average laboratory is hardly possible and, in view of the other applications of the equipment, of questionable value.

6. Special threshold measurements

One of the valuable features of the Békésy audiometer with electronic signal level control set up using Brüel and Kjaer equipment (or comparable) is the case of conversion of the dynamic scale of the recording. For the system described here, this conversion can be achieved by changing of the recording

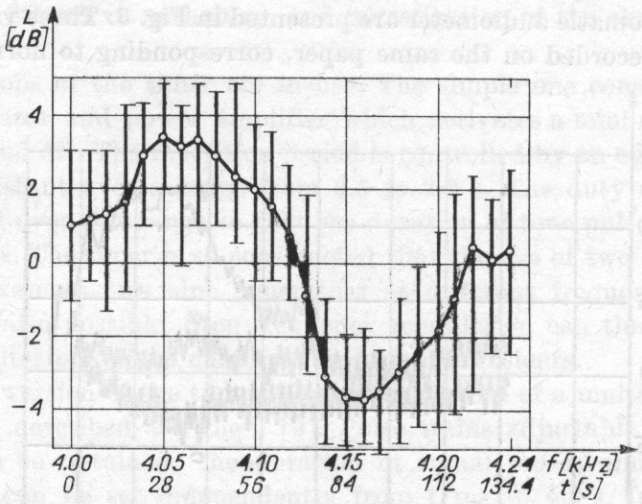

Fig. 4. Threshold audiogram determined from 25 experimental tracings for the same subject (Investigation of diplacusis binauralis [3])

Median values and interquartiles for 25 threshold tracings taken at equal frequency increments, rate of level control – 3 dB/s, recording potentiometer – 10 dB, paper speed – 1 mm/s, lower limiting frequency – 200 Hz, writing speed – 100 mm/s

potentiometer in the 2305 level recorder. The full dynamic scale of the record may thus be chosen to equal 10, 25, 50 or 75 dB.

In normal practice a 75-dB scale is commonly used which allows the tracing both of quite considerable hearing loss and of normal hearing, with sufficient accuracy.

Recording scales narrower than 75 dB, particularly 10 dB and 25 dB, have proved to be very useful for more accurate investigation of the threshold curves over a limited frequency range and/or at constant frequency. Limitation of the frequency range to the range of particular interest, results from the

obvious fact that for accurate tracing of the threshold curve, the rate of automatic frequency scanning must be sufficiently low. At such low rates of frequency scanning the tracing of the whole auditory range would be greatly prolonged and could result in tracing errors due to fatigue.

Tracing of the threshold curves with increased accuracy can be applied to the investigation of, for example, diplacusis binauralis (an anomalous threshold affecting the perception of pitch). An illustrative example of the usefulness of such tracings is the audiogram presented in Fig. 4, obtained with 10 dB recording potentiometer in the 4.0 to 4.25 kHz frequency range. This audiogram resulted from 25 separate audiometric tracings obtained from one listener (right ear). Circles in the diagram represent median value and vertical lines the interquartiles. Median values were taken at equal time and frequency increments.

To determine the significance of the threshold level variations observed in the experiment, particularly in view of the considerable dispersion of the results, control measurements were also performed. In the control series, the threshold tracing were obtained from the same listener (the same ear, control tracings run immediately after the experimental tracings) following the same procedure as in the experimental series. However, the automatic frequency scanning was disconnected and the frequency set to 4.0 kHz. The

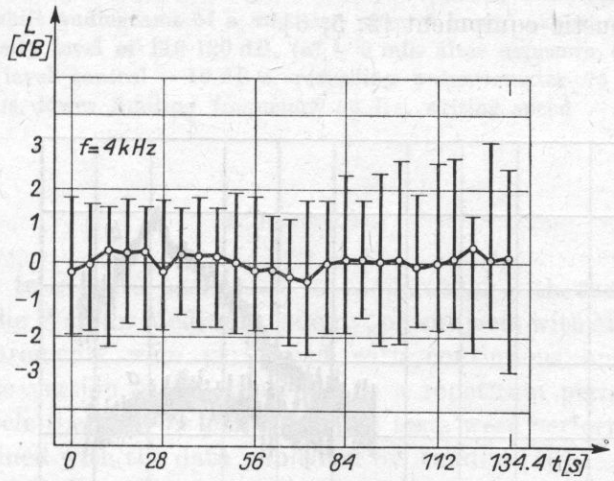

Fig. 5. Threshold audiogram determined from 25 control tracings as in Fig. 4. (Investigation of diplacusis binauralis [3]). Setting of audiometer controls as in Fig. 4

duration of each of the 25 control tracings was the same as in the exper mental tracings and amounted to 140 s. The results obtained from the control runs are presented in Fig. 5.

The results presented in Figs. 4 and 5 demonstrate well the degree of accuracy which can be achieved by using the system described and by averaging the results. The curve in Fig. 4, representing a fraction of the hearing

threshold, shows distinct hearing loss near 4.05 kHz and some supranormal hearing in the region of 4.15 kHz. The measurements of the other (left) ear in the same listener resulted in a flat threshold curve to within ± 1 dB.

In the threshold curves presented in Figs. 4 and 5 a small discrepancy between the threshold levels at 4 kHz is observed. It seems probable that this discrepancy may have resulted from the procedure applied in the experiment, namely from running the whole of the experimental measurements and then the whole of the control measurements rather than alternating them. Some small change of the threshold criterion in the subject could have introduced the observed constant error of about 1 dB.

7. Temporary threshold shift measurements

In industrial audiometric tests, concerning the hazards of hearing loss in employees exposed to high intensity sounds, it often appears necessary to determine the amount of temporary threshold shift (TTS) as quickly as possible. Such data are used for the determination of the risks of hearing loss and eventually for the determination of permissible daily exposures, or a reduction of dangerous exposures [11, 12]. Similar hazards of hearing loss are observed also in musicians, particularly those performing rock-and-roll music using high power electroacoustic equipment [2, 5, 6].

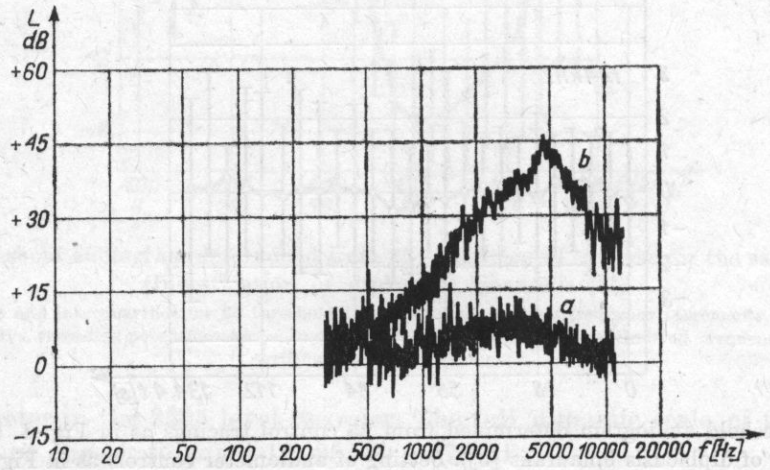

Fig. 6. Threshold audiograms before (a), and 9 min after exposure (b) to shock sound at 130 dB SPL; rate of level control — 10 dB/s, recording potentiometer — 75 dB, paper speed —0.3 mm/s, lower limiting frequency — 200 Hz, writing speed — 250 mm/s

Examples of the TTS tracings obtained in various conditions are presented in Figs. 6 and 7. In Fig. 6 the threshold audiograms before and after exposure to shock sound at about 130 dB SPL and characterized by almost uniform

spectrum density over the auditory range is given. The threshold audiograms in Fig. 7 were obtained from the musician after 4 hours' performance in the ⟪Hybrydy⟫ students' club dance hall, where the high power electroacoustic system gave a peak intensity of 110 to 120 dB.

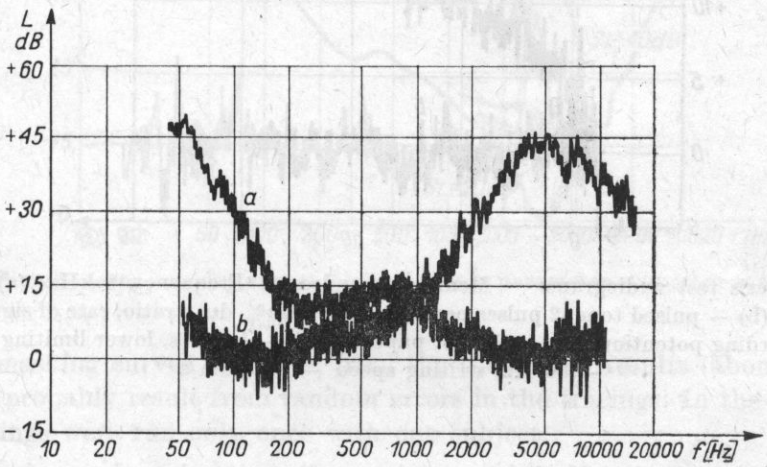

Fig. 7. Threshold shift audiograms of a musician after 4 hours' exposure to rock-and-roll music at an intensity level of 110-120 dB, (a) — 9 min after exposure, (b) — 96 hrs after exposure; rate of level control — 10 dB/s, recording potentiometer 75 dB, paper speed — 0.3 mm/s, lower limiting frequency 50 Hz, writing speed — 250 mm/s

8. Jerger's test

The Jerger tests were performed in cooperation with the Dept. of Otolaryngology of the Warsaw Medical Academy, on subjects with Menière's syndrome. The measurements were performed with continuous and pulsed tones using the simple version of the timer set to a repetition period of 0.5 s and a 50% duty cycle (i.e. 250 ms pulses). These tests were performed to compare the results obtained with the data published by JERGER [10].

In fact the results showed some diagnostic significance for this method. The threshold audiogram from one of the subjects with Menière's, obtained at a constant frequency, is presented in Fig. 8 as an example.

It seems worth pointing out that this type of Békésy tracing was observed in subjects with Menière's syndrome only in the high frequency region of the auditory range, and only in subjects with a hearing loss of at least 20 to 30 dB in that frequency region, mostly at frequencies corresponding to the maximum hearing loss. In the other cases investigated the differences observed between the continuous and pulsed tone tracings were less pronounced or undetected.

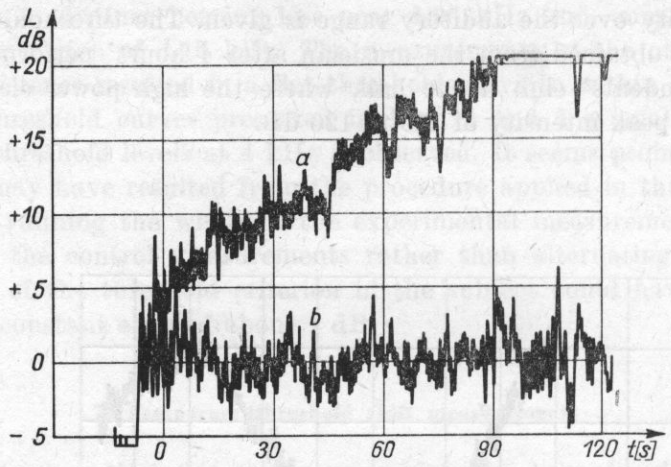

Fig. 8. Jerger's test audiograms — Menière's syndrome. Frequency 8 kHz: (a) — continuous tone, (b) — pulsed tone, 2 pulses per second at a 50% duty ratio, rate of signal control 3 dB/s, recording potentiometer — 25 dB, paper speed — 1 mm/s, lower limiting frequency — 50 Hz, writing speed — 100 mm/s

It would seem that further research on a large number of cases is necessary to evaluate the significance of this method for diagnostic purposes.

9. Masking measurements

Masking methods in psychoacoustics and in audiometry can be divided into two classes i.e. simultaneous masking, and per and post stimulatory masking.

In simultaneous masking various methods based on the use of continuous (as a function of time) stimuli, pulse stimuli or their combinations are known. In per and post stimulatory masking pulse stimuli are used as a rule.

The simplification of experimental procedure which results from the possibility of automatic signal level control, automatic frequency scanning and automatic tracing and recording of the signal level is unquestionable. This seems to be evident in masking experiments from the large number of papers published over the last decade in which Békésy tracings in classic or modified form were used [8].

To illustrate the usefulness of automatic audiometry in the investigation of simultaneous masking, typical masking curves for a 3 kHz sinusoidal signal at various sensation levels, obtained using the system described (without threshold equalizer) are presented in Fig. 9. Each circle on the diagram corresponds to the average level recorded at the appropriate frequencies. The tracings had at least 100 threshold crossings (spikes) and lasted about 120 s each. The rate of level control was 3 dB/s. Some small discrepancies observed at the

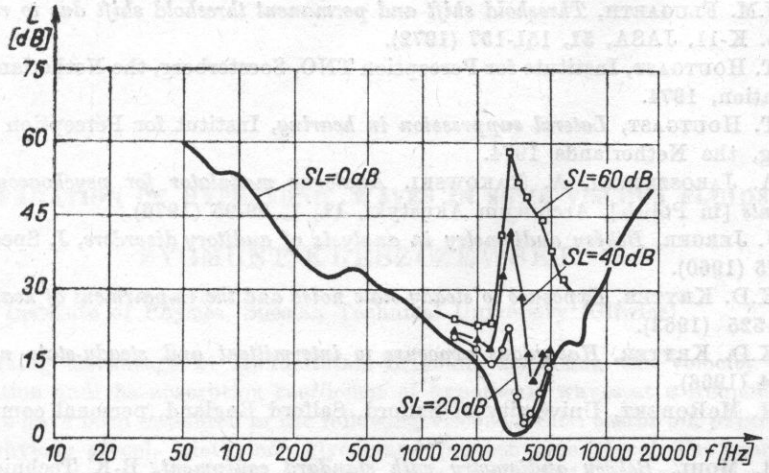

Fig. 9. Simultaneous masking curves for 3 kHz tone; parameter — masker sensation level

tops of masking curves in Fig. 9, from the theoretical results (about 2 dB difference) probably result from random errors in the tracings. In the case shown the tracings were run only once with one subject.

10. Conclusion

A Békésy audiometer constructed from conventional Brüel and Kjaer laboratory equipment and some specially designed additional units has now been in use for over 6 years. It can be used in a number of applications in hearing threshold measurements and in the other psychoacoustical measurements.

The possibility of conversion of the recording scale, the possibility of using pulse signals of varying character from the external units (described elsewhere), and the automatic averaging of the tracings by suitable adjustment of the 2305 controls, have been shown to be particularly useful.

References

[1] Z. Bochenek, K. Janczewski, B. Kalinowski, *Békésy audiometry in the skull after-injure cases* [in Polish], Otolaryngologia polska, **22**, 3, 413-419 (1968).

[2] E. Bohdanowicz, *Rock and roll music and the hearing impairment in performers* [in Polish], unpublished Master's thesis, Academy of Music, Laboratory of Musical Acoustics, Warszawa 1972.

[3] A. Jaroszewski, unpublished data, Report U-73, Archives, Laboratory of Musical Acoustics, Academy of Music, Warszawa 1973.

[4] H. Fastl, Institut für Elektroakustik der TU, München, personal communication, 1975.

[5] J. M. Flugarth, *Modern day rock and roll music and damage risk criteria*, JASA, **45**, 704-711 (1969).

[6] J.M. FLUGARTH, *Threshold shift and permanent threshold shift due to rock and roll music*, pap. K-11, JASA, **51**, 151-157 (1972).

[7] T. HOUTGAST, Institute for Perception TNO, Soesterberg, the Netherlands, personal communication, 1974.

[8] T. HOUTGAST, *Lateral suppression in hearing*, Institut for Perception TNO, Eds., Soesterberg, the Netherlands 1974.

[9] A. JAROSZEWSKI, A. RAKOWSKI, *Analogue modulator for psychoacoustical pulse measurements* [in Polish], Archiwum Akustyki, **11**, 1, 89-95 (1976).

[10] J. JERGER, *Békésy audiometry in analysis of auditory disorders*, J. Speech Hearing Res., 3, 275 (1960).

[11] K.D. KRYTER, *Exposure to steady-state noise and the impairment of hearing*, JASA, **35**, 1515-1525 (1963).

[12] K.D. KRYTER, *Hazardous exposure to intermittent and steady-state noise*, JASA, **39**, 451-464 (1966).

[13] H. MCROBERT, University of Salford, Salford England, personal communication, 1969.

[14] B. MOHL, *Békésy audiometry with standard equipment*, B-K Technical Rev., 1 (1973).

[15] A. RAKOWSKI, A. JAROSZEWSKI, T. ŁĘTOWSKI, *Békésy's audiometer with standard laboratory equipment* [in Polish], Arch. Akustyki, **4**, 3, 247-262 (1969).

[16] A. RAKOWSKI, A. JAROSZEWSKI, T. ŁĘTOWSKI, *Automatic audiometer* [in Polish], Pat. PRL No 138238.

[17] E. ZWICKER, R. FELDTKELLER, *Das Ohr als Nachrichten empfanger*, S. Hirzel Verlag, 1967 (Bild 18.3, p. 54).

Received 25th September 1975

ARCHIVES OF ACOUSTICS
1, 3, 243-253 (1976)

PROPAGATION OF HYPERSONIC WAVES IN SOME VISCOUS FLUIDS

ZYGMUNT KLESZCZEWSKI

Institute of Physics, Silesian Technical University (Gliwice)

Taking advantage of Mandelsztam-Brillouin dispersion the velocity of propagation and the absorption coefficient of hypersonic waves at a frequency of 8 GHz have been measured in the following viscous fluids: castor oil, paraffin oil, diethylene glycol, triethylene glycol and polyethylene glycol. The results obtained are discussed on the basis of relaxation theory and ISAKOVICH-CZABAN theory.

1. Introduction

An analysis of the results of measurements of the velocity of propagation and the absorption coefficient of hypersonic waves in very viscous fluids [4, 5, 8, 9] leads to the conclusion that relaxation theory [6] cannot be applied to them since there is considerable divergence between the experimental data and theoretical predictions. In the hypersonic region this divergence is even more conspicuous. However, the range of experimentation at very high frequencies is relatively small because of unfavourable conditions and this hinders comparison between theory and experiment.

By virtue of the very high absorption, the only proper method of investigating the propagation of hypersonic waves in very viscous fluids is an examination of the spectrum of molecular light diffusion. As a result of the scattering of photons by thermal phonons there appear, in the spectrum of scattered light, components of changed frequency, the so called Mandelsztam-Brillouin components [1]. The vibration frequencies of these components are shifted relative to the primary light frequency by an amount given by the formula

$$f = 2nf_0 \frac{v}{c} \sin\frac{\theta}{2}, \tag{1}$$

where f_0 is the primary frequency of the light wave, n — coefficient of light refraction, v — velocity of hypersonic wave, c — velocity of light, θ — scattering angle.

The absorption of hypersonic waves which always occurs in a medium causes a certain broadening of components of the fine structure

$$\delta\nu = \frac{\alpha v}{\pi c}, \tag{2}$$

where $\delta\nu$ denotes the half width expressed in wave numbers, and α the coefficient of absorption of hypersonic wave.

Thus, if we measure the distance between the fine structure components and their half widths, we can evaluate from formulae (1) and (2) the velocity of propagation and the coefficient of absorption of the hypersonic waves.

In this paper — by taking advantage of this method — the velocity of propagation and absorption coefficient of hypersonic waves in castor oil, paraffin oil, di-, tri- and polyethylene glycol have been measured. The in measurements were made at a frequency of 8 GHz in the temperature interval from —40 to 90°C. To obtain more extensive information, measurements in the ultrasonic region, at a frequency of 3 MHz, were also made. The results obtained will be discussed on the basis of existing theories of the propagation of waves in fluids.

2. System for examination of the fine structure components

Fig. 1 shows the measuring system. The ligt source is a ruby laser with $\lambda = 6943$ Å; pulse power $M = 100$ MW; time of duration $t = 3 \times 10^{-8}$ s. The half width of the emission line was smaller than 0.01 cm^{-1}. The laser light wa

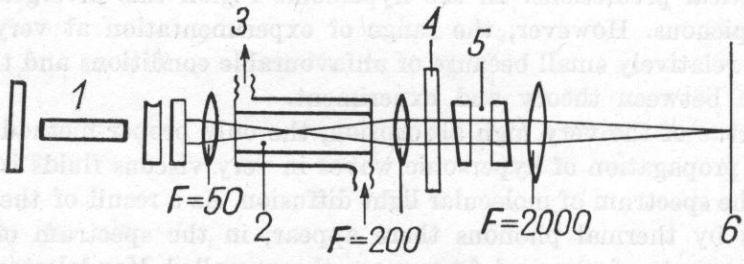

Fig. 1. Diagram of the Mandelsztam-Brillouin testing system
1 — ruby laser, 2 — vessel containing tested liquid, 3 — cooling, 4 — mat plate, 5 — Fabry-Perot interferometer, 6 — photographic film

ocused by means of a lens of focal length $f = 5$ cm, in a vessel containing thef fluid to be tested. The vessel had a length $l = 200$ mm, and a diameter $d = 40$ cm. The purity of the fluids to be tested was determined by measurement of the coefficient of light refraction, density and viscosity. The measurement results are given in Table 1.

The spectrum of scattered light was analyzed with the aid of a Fabry-Perot interferometer IT51-30. The distance between interferometer mirrors was 0.6 cm, and this corresponds to the scatter region $\delta\nu = 0.83$ cm^{-1}. A chamber with a focal length of $f = 2015$ mm produced an image on the photographic

Table 1. Density, refraction coefficient and viscosity of tested fluids ($t = 20°C$)

Substance	$\varrho\left[\frac{g}{cm^3}\right]$	n	η [poise]
Paraffin oil	0.807	1.4421	2.21
Castor oil	0.963	1.4490	8.85
Diethylene glycol	1.118	1.4475	0.63
Triethylene glycol	1.127	1.4578	0.83
Polyethylene glycol	1.203	1.4621	0.92

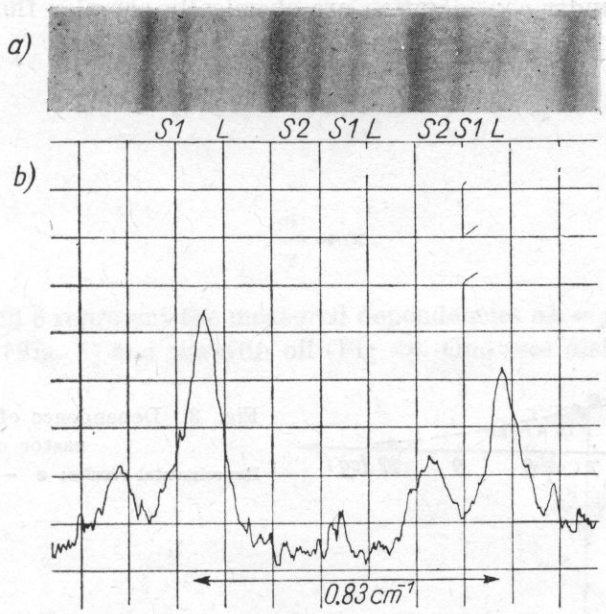

Fig. 2. Spectrum of the fine structure of the light dispersion line in triethylene glycol: a) Fabry-Perot interferogram, b) microphotogram
L – laser radiation, *S*1, *S*2 – stokes components

plate. The linear dispersion was of the order 10^7. All measurements were made at the angle of 180°. The accuracy of measurement was approximately two seconds of arc. The photographs obtained were analyzed by means of a microphotometer. Fig. 2 shows an example of the lines of the fine structure obtained.

3. Results and discussion of the measurements

An analysis of the dependence of the absorption coefficient in the ultra-hypersonic region in castor and paraffin oil points to departures from a relaxation theory with one or two times of relaxation and a complexity of relaxation processes. Figs. 3 and 4 show the dependence of α/f^2 on $\log f$ for the above mentio-

ned oils. Within the whole frequency region a square dependence of absorption coefficient is not observed. The curves of α/f^2 all have almost uniform slope, without points of inflexion which would have been indicative of a determined time of relaxation for a given mechanism. We should rather consider a superposition of a great number of relaxation processes, both of shear and volumetric viscosity over a wide range of frequencies. Evidence for the occurrence of volumetric viscosity relaxation is given by the fact that at frequencies above 10 MHz the total absorption coefficient for both oils is smaller than the value of this coefficient in stokes. The calculation of these relaxation times, as also the explanation of their molecular system is very difficult especially because the substances under consideration are chemically complex fluids that possess molecules of various sizes and shapes.

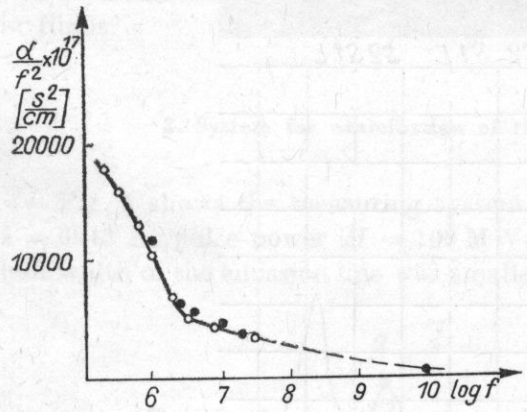

Fig. 3. Dependence of α/f^2 on $\log f$ for castor oil
Experimental results: ● – by author, ○ – [7]

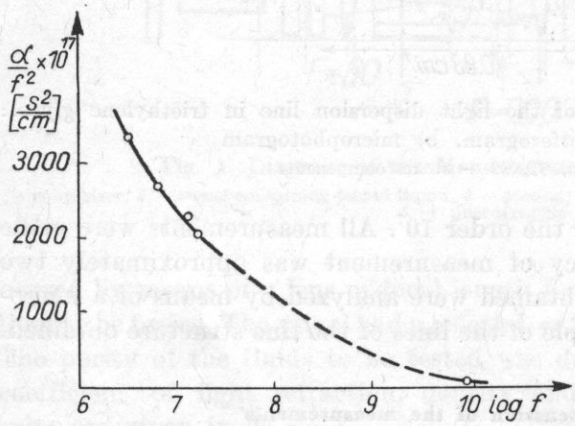

Fig. 4. Dependence of α/f^2 on $\log f$ for paraffin oil

It is worth noting that the maximum of the curve $\alpha\lambda$ as a function of τ should occur for $\tau = 1/\omega$, i.e. at a point at which the dependence of α/τ versus τ is reduced to a half of its maximum value. This is the result of the following considerations.

The value of a/τ — according to relaxation theory — is given by the formula

$$\frac{a}{\tau} = \frac{\omega^2 (v_\infty^2 - v_0^2)}{(1 + \omega^2 \tau^2) \cdot 2 v_0^3}, \tag{3}$$

where τ is the time of the relaxation, v_0 and v_∞ the velocities of wave propagation at very small and infinitely large frequencies respectively.

Depending on the value of $\omega\tau$ the formula can take various forms:

for $\omega\tau \ll 1$

$$\frac{a}{\tau} = \frac{\omega^2 (v_\infty^2 - v_0^2)}{2 v_0^3}, \tag{4}$$

for $\omega\tau = 1$

$$\frac{a}{\tau} = \frac{\omega^2 (v_\infty^2 - v_0^2)}{4 v_0^3}, \tag{4a}$$

for $\omega\tau \gg 1$

$$\frac{a}{\tau} \to \infty. \tag{4b}$$

Figs. 5 and 6 represent the measured dependencies $a\lambda = f(\tau)$ and $a/\tau = f(\tau)$ for castor oil (Fig. 5) and paraffin oil (Fig. 6). One sees distinctly the shift of

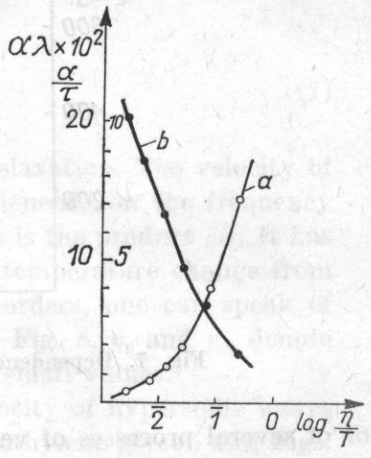

Fig. 5. Dependence of $a\lambda$ (a) and a/τ (b) on log η/T for castor oil

the maximum of the curve towards higher values of τ for both fluids. At the same time it is assumed, as is often the case, that the time of relaxation is proportional to the viscosity and inversely proportional to temperature,

$$\tau = B \frac{\eta}{T}, \tag{5}$$

where B is a constant.

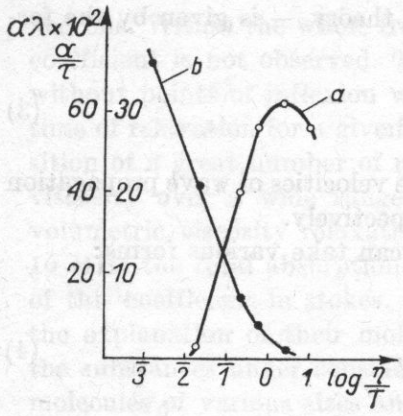

Fig. 6. Dependence of $\alpha\lambda$ (a) and α/τ (b) on $\log \eta/T$ for paraffin oil

The frequency dependence of the absorption coefficient for triethylene glycol (Fig. 7) is similar to that for castor and paraffin oil. However, it should be noted that for frequencies $f < 15$ MHz the curve is very steep, and this may indicate the appearance in this area of relaxation process of duration $\tau = 10^{-7}$s

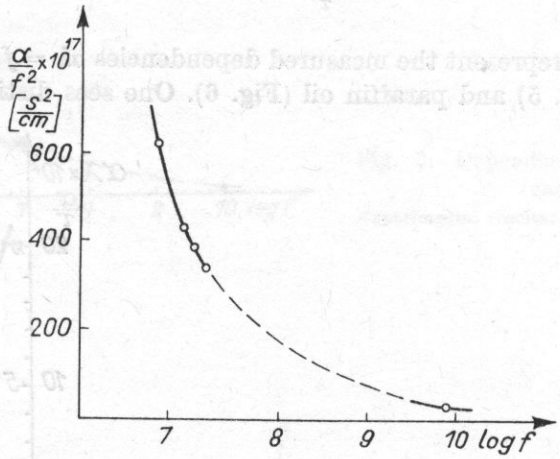

Fig. 7. Dependence of a/f^2 on $\log f$ for triethylene glycol

or of several processes of very similar relaxation times. Above a frequency of 8 MHz, the total absorption coefficient is smaller than the values expressed in stokes, thus already at this frequency shear viscosity relaxation occurs.

Velocity measurements as a function of temperature, both in ultra- and hypersonic regions, are very interesting for many reasons. The dependence of the velocity of ultrasonic waves on the temperature in paraffin o l ($f = 3$ MHz) is shown in Fig. 8. At the first sight it seems that this curve is a curve of the relaxation type. However, a thorough analysis of this dependence indicates that this conclusion is inaccurate.

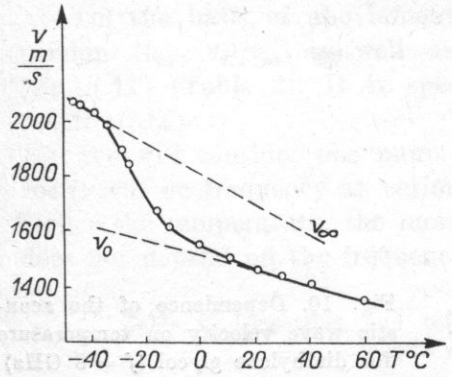

Fig. 8. Dependence of the acoustic wave velocity on temperature for paraffin oil ($f = 3$ MHz)

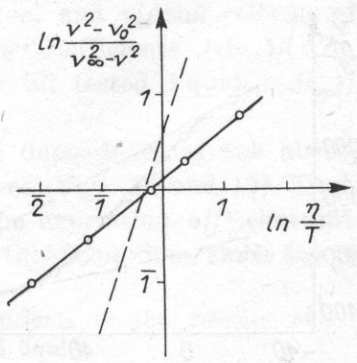

Fig. 9. Dependence of $\ln (v^2 - v_0^2)/(v_\infty^2 - v^2)$ on $\ln \eta/T$ for paraffin oil

The discussion will use the well-known formula of relaxation theory

$$\frac{v^2 - v_0^2}{v_\infty^2 - v^2} = \omega^2 \tau^2. \tag{6}$$

In Fig. 9 this dependence is shown by means of a broken line. Experimental data are presented by dots. They arrange themselves with good accuracy on the curve

$$\frac{v^2 - v_0^2}{v_\infty^2 - v^2} = \omega\tau, \tag{7}$$

but this does not result clearly from the theory of relaxation. The velocity of acoustic waves (as does the absorption coefficient) depends on the frequency and on the temperature. In fact, in all formulae there is the product $\omega\tau$. It has already been stated that $\tau \sim \eta/T$. Thus if, with the temperature change from $-30°$C, the viscosity would have changed by four orders, one can speak of very high and very low frequencies for this case. In Fig. 8, v_0 and v_∞ denote only extrapolated velocities for very large and very small values.

Figs. 10 and 11 show the dependence of the velocity of hypersonic waves as a function of temperature for diethylene and polyethylene glycol, and Figs. 12 and 13 the dependence of $\log(v^2 - v_0^2)/(v_\infty^2 - v^2)$ on $\log \eta/T$. When making hypersonic measurements by Brillouin scatter method, a change in temperature also (slightly) changes the frequency. However, because of very large changes in the value of τ, ω can be assumed constant to a good approximation. For these liquids too there occurs great divergence from the predictions of relaxation theory. Broken lines in Figs. 12 and 13 represent the dependence $(v^2 - v_0^2)/(v_\infty - v^2) = \omega^2\tau^2$ (relaxation theory). The experimental points, as for paraffin oil, arrange themselves on the straight line $(v^2 - v_0^2)(v_\infty^2 - v^2) = \omega\tau$.

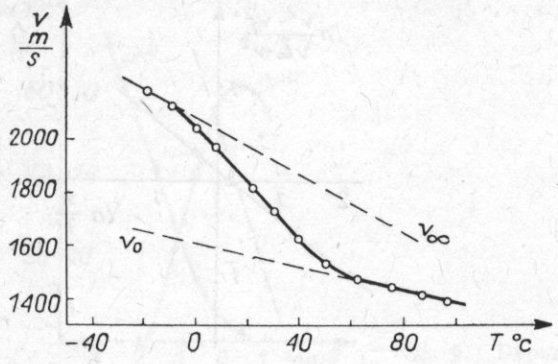

Fig. 10. Dependence of the acoustic wave velocity on temperature for diethylene glycol ($f = 8$ GHz)

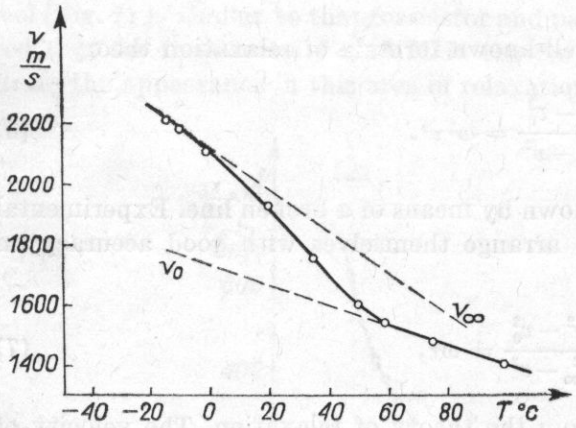

Fig. 11. Dependence of the acoustic wave velocity on temperature for polyethylene glycol ($f = 8$ GHz)

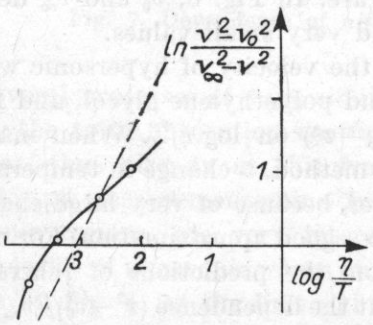

Fig. 12. Dependence of $\ln (v^2 - v_0^2)/(v_\infty^2 - v^2)$ on $\log \eta/T$ for diethylene glycol

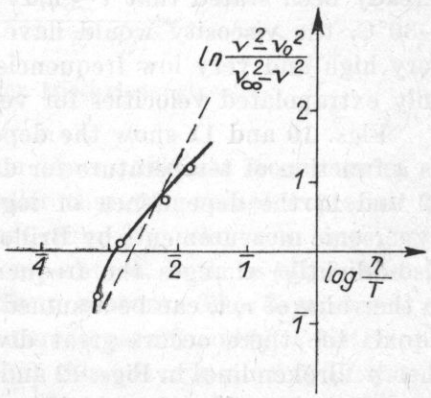

Fig. 13. Dependence of $\ln (v^2 - v_0^2)/(v_\infty^2 - v^2)$ on $\log \eta/T$ for polyethylene glycol

On the basis of above-mentioned values v_0 and v_∞ the velocity of dispersion $(v_\infty - v_0)/v_\infty$ as well as temperature coefficients $(\Delta v_\infty)/(\Delta T)$ and $(\Delta v_0)/(\Delta T)$ (Table 2). It is specific that for all tested liquids $(\Delta v_\infty)/(\Delta T) > (\Delta v_0)/(\Delta T)$.

We will consider one more form for the dependence of the absorption coefficient on frequency at various temperatures (Figs. 14 and 15). Thus, the higher the temperature, the more nearly is the expression α/f^2 constant and does not depend on the frequency. However, this is obvious since the higher

Table 2. Dispersion and temperature coefficients of the velocity of acoustic waves for tested liquids

Substance	$\frac{v_\infty - v_0^2}{v_0}$	$\frac{\Delta v_\infty}{\Delta T}\left[\frac{\text{m}}{\text{s deg}}\right]$	$\frac{\Delta v_0}{\Delta T}\left[\frac{\text{m}}{\text{s deg}}\right]$
Paraffin oil	0.28	−5.4	−2.1
Diethylene glycol	0.26	−5.8	−2.3
Polyethylene glycol	0.19	−7.0	−3.3

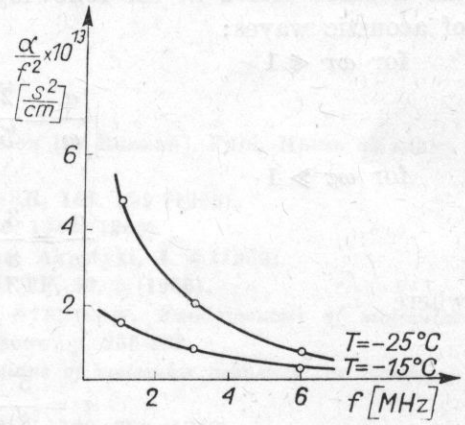

Fig. 14. Dependence of α/f^2 on frequency for triethylene glycol at various temperatures

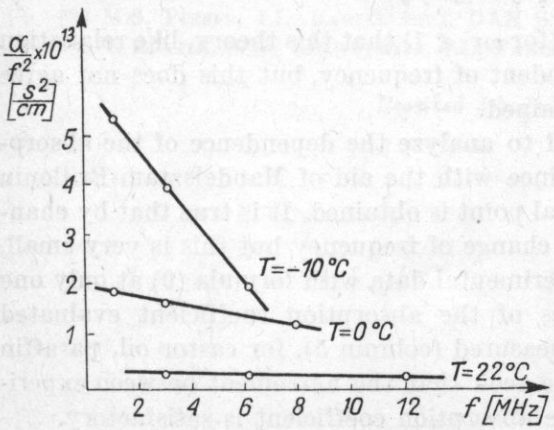

Fig. 15. Dependence of α/f^2 on frequency for paraffin oil at various temperatures

the temperature, the less viscous the fluid becomes. It can therefore be expected that the formulae of relaxation theory will be satisfied since the latter predicts that α/f^2 does not depend on frequency.

At present the most authoritative theory of acoustic wave propagation in fluids of high viscosity is regarded to be the theory developed by ISAKOVICH and CZABAN [2, 3], also called non-local theory.

At the root of this theory lies the assumption that a viscous fluid is an inhomogeneous two-phase medium. Each of the phases of this medium has, apart from normal thermodynamic parameters, two more parameters which determine the concentration of holes. At equilibrium the concentration for both phases is equal. The motion of an acoustic wave causes disturbance of the medium, and thus also the change of parameters that determine the concentration of holes. The return to equilibrium is effected by a diffusion of holes, the time of which depends on the diffusion coefficient and the size of the phase with the smaller concentration of holes. A retarded return of the medium to the state of equilibrium relative to the change in ultrasonic wave pressure causes the absorption and dispersion of sound velocity. Having justified the above assumptions, the authors arrive at the following expression for the absorption coefficient of acoustic waves:

for $\omega\tau \ll 1$

$$\frac{\alpha}{\omega} = \frac{2}{5} \frac{\omega\tau(v_\infty^2 - v_0^2)}{v_0^2 - v_\infty}; \tag{8}$$

for $\omega\tau \gg 1$

$$\frac{\alpha}{\omega} = \frac{3}{8} \frac{v_\infty^2 - v_0^2}{v_0^2 - v_\infty} \frac{1}{\sqrt{\omega\tau}}, \tag{9}$$

where

$$\tau = \frac{5}{3} \frac{v_\infty^2}{\varrho v_0^2} \frac{\eta + \frac{3}{4}\eta}{v_\infty^2 - v_0^2}.$$

It can be seen from formula (8) (for $\omega\tau \ll 1$) that this theory, like relaxation theory, assumes that α/f^2 is independent of frequency, but this does not agree with the experimental results obtained.

For high frequencies, it is hard to analyze the dependence of the absorption coefficient on the frequency since with the aid of Mandelsztam-Brillouin scatter method only one experimental point is obtained. It is true that by changing the temperature, we can get a change of frequency but this is very small. It was thus possible to compare experimental data with formula (9) at only one frequency. Table 3 contains values of the absorption coefficient evaluated from formula (9) (column 4), and measured (column 5), for castor oil, paraffin oil and triethylene glycol. It can be seen that the agreement between experimental and theoretical values of the absorption coefficient is satisfactory.

Table 3. Theoretical and experimental values of absorption coefficient of hypersonic waves

Substance	T[°C]	$f\times10^{-9}$[s^{-1}]	$\alpha\times10^{-3}$ (theory) [cm^{-1}]	$\alpha\times10^{-3}$ (exp.) [cm^{-1}]
Castor oil	20	8.20	5.3	24
Paraffin oil	20	7.71	24	20
Triethylene glycol	20	8.46	15	21

It can be concluded that the theory of Isakovich and Czaban assumes that the ratio $(v^2-v_0^2)/(v_\infty^2-v^2)$ is proportional to $\omega\tau$, and that this is in agreement with the experimental results described above. Similar conclusions can also be draw from reference [10] where the velocity of propagation of hypersonic waves in glyceril triacetate and propylene glycol has been measured using the Mandelsztam-Brillouin method of forced dispersion. Thus, it seems that the theory of Isakovich and Czaban in the region of high frequencies yields results in good agreement with experiment, whereas at lower frequencies considerable discrepancies occur.

References

[1] I.L. Fabieliński, *Molecular light dispersion* [in Russian], Publ. House «Nauka» Moscow 1965, p. 82-89, 285-324, 440-448.

[2] M.A. Isakowich, I.A. Czaban, DAN SSSR, **165**, 299 (1965).

[3] M.A. Isakowich, I.A. Czaban, ZETF, **50**, 1343 (1966).

[4] Z. Kleszczewski, A. Opilski, Archiwum Akustyki, **4**, 4 (1969).

[5] S.W. Kriwochiża, I.L. Fabielińskij, ZETF, **50**, 3 (1966).

[6] I.G. Michajłow, B.A. Sołowiew, P. Syrmikow, *Fundamentals of molecular acoustics* [in Russian], Publ. House «Nauka», Moscow, p. 235-282.

[7] I.G. Michajłow, L.I. Sawina, *Applications of molecular acoustics* [in Russian], MOPI, vol. **4** (1957), p. 85-93.

[8] M.S. Piesin, I.L. Fabieliński, DAN SSSR, **129**, 299 (1959).

[9] M.S. Piesin, I.L. Fabieliński, DAN SSSR, **135**, 114 (1960).

[10] I. Zlatin, S.W. Kriwochiża, I.L. Fabieliński, ZETF, **56**, 4, 1186 (1969).

Received 5th July 1975